Directional singularity escape and avoidance for single-gimbal control moment gyroscopes

Valk, Laurens; Berry, Andrew; Vallery, Heike

DOI
10.2514/1.G003132

Publication date
2018

Document Version
Accepted author manuscript

Published in
Journal of Guidance, Control, and Dynamics

Directional Singularity Escape and Avoidance for Single-Gimbal Control Moment Gyroscopes *†

Laurens Valk‡, Andrew Berry§, and Heike Vallery¶
Delft University of Technology, Delft, 2628 CD, The Netherlands

Despite the long history of studies on the singularity problem inherent to single-gimbal control moment gyroscopes, few existing gimbal steering laws can both accurately track moments and escape or avoid every type of singularity. The most-referenced steering laws perturb the system suboptimally at every singularity to enforce escape, which creates a tradeoff between minimizing escape time and minimizing transient tracking errors and gimbal rates. It is shown that no such tradeoff is necessary by proposing new singularity measures to quantify the current and future reference moment tracking capabilities and defining explicitly how an anticipated singularity can be avoided or escaped. Using these measures to separate and prioritize the tasks of moment tracking, gimbal damping, and singularity escape and avoidance, a gimbal steering law is designed that accurately tracks moments and avoids singularities when possible while escaping them with a minimal error moment otherwise. The steering law has smaller overall tracking errors and lower peak gimbal rates, and it achieves singularity escape faster than existing methods, as demonstrated analytically and using simulations.

Nomenclature

n	Number of single-gimbal control moment gyroscopes
m	Nominal output moment dimension
i	Gimbal index
j	Singular component index
t	Time
$\mathbf{0}_n$, $\boldsymbol{I}_n$	$n \times n$ zero and identity matrix
γ_i, $\dot{\gamma}_i$, Ω_i	i-th gimbal angle, gimbal rate, and flywheel rate
$\hat{\boldsymbol{f}}_i$, $\hat{\boldsymbol{g}}_i$, $\hat{\boldsymbol{h}}_i$	i-th gimbal frame unit vectors
$\boldsymbol{F}$, $\boldsymbol{G}$, $\boldsymbol{H}$	$m \times n$ matrices of gimbal frame vectors
$\boldsymbol{S}$, $\boldsymbol{U}$, $\boldsymbol{V}$	Singular value decomposition matrices of $\boldsymbol{F}$
σ_j, $\hat{\boldsymbol{u}}_j$, $\hat{\boldsymbol{v}}_j$	j-th singular value and vectors of $\boldsymbol{F}$
$\hat{\boldsymbol{s}}$	Singular direction
$\boldsymbol{F}^{\circ}$, α	Filtered pseudoinverse of $\boldsymbol{F}$, damping factor α
$\dot{\boldsymbol{\gamma}}$, $\dot{\boldsymbol{\gamma}}_c$	Actual and commanded gimbal rates
$\dot{\boldsymbol{\gamma}}_p$, $\dot{\boldsymbol{\gamma}}_e$	Pseudoinverse and escape components of $\dot{\boldsymbol{\gamma}}_c$
$\dot{\boldsymbol{\gamma}}_s$, $\boldsymbol{\theta}$	Secondary task gimbal rates and directions
$\mathbb{I}$, $\emptyset$	Set of anti-saturated gimbals and empty set
$\boldsymbol{\rho}$, $\boldsymbol{\omega}$	Satellite attitude and angular velocity
$\boldsymbol{M}_{\text{ext}}$	External moment acting on whole satellite
$\boldsymbol{M}_{\text{int}}$	Moment between satellite body and gyroscopes
$\boldsymbol{M}_{...}$	Other moments to evaluate equations of motion
$\boldsymbol{J}_{...}$	Inertia parameters
$\boldsymbol{M}_d$	Gyroscopic moment due to satellite rotation
$\boldsymbol{\tau}$, $\boldsymbol{\tau}_c$	Gyroscopic moment due to $\dot{\boldsymbol{\gamma}}$ or $\dot{\boldsymbol{\gamma}}_c$
$\boldsymbol{\tau}_s$	Gyroscopic moment due to $\dot{\boldsymbol{\gamma}}_s$
$\boldsymbol{\tau}_{\text{ref}}$, $\boldsymbol{e}$	Gyroscopic moment reference and error
J, $\boldsymbol{P}$, $\boldsymbol{Q}$	Cost function and weighing matrices
Ω_c, μ	Rate and momentum magnitude of one flywheel
$\boldsymbol{b}_i$	Projection of $\hat{\boldsymbol{\tau}}_{\text{ref}}$ on plane orthogonal to $\hat{\boldsymbol{g}}_i$
ψ_i	Angle between $\hat{\boldsymbol{h}}_i$ and $\boldsymbol{b}_i$
p_i, d_i	Gimbal potential and escape potential
δ_{man}	Manipulability measure
δ_{track}, δ_{pot}	Tracking index and total gimbal potential
z_j, κ_j	Tracking index parameters
σ_{min}	Singular value below which damping is applied
σ_{acp}	Singular value for tracking with acceptable rates
$k_{\dot{\gamma}}$, k_{Ω}	Gimbal and flywheel motor gains
$\dot{\boldsymbol{\omega}}_c$	Body acceleration for computing motor torques
β, k_p, k_v	Satellite and attitude control constants
τ_{min}, τ_{max}	Minimum and maximum moment magnitude
η, d_0, ζ	DSEA control parameters
λ, ϕ, ϵ, W_i	o-DSR control parameters
RA	Left superscript denoting evaluation at nearest reference-aligned singularity

*This author's version corresponds to the accepted manuscript without complete editing and formatting. Please refer to the published version before citing: Valk, L., Berry, A., and Vallery, H., "Directional Singularity Escape and Avoidance for Single-Gimbal Control Moment Gyroscopes," *Journal of Guidance, Control, and Dynamics*, Vol. XX, No. XX, XX–XX. 2018, doi: 10.2514/1.G003132

†Submitted 20 June 2017; revision submitted 14 November 2017; accepted for publication 15 November 2017; published online 10 January 2018.

‡M.Sc. Student, TU Delft Robotics Institute, laurensvalk@gmail.com.

§Ph.D. Student, TU Delft Robotics Institute, a.berry@tudelft.nl.

¶Professor, TU Delft Robotics Institute, h.vallery@tudelft.nl.

I. Introduction

Single-gimbal control moment gyroscopes (SGCMGs) are powerful actuators capable of imparting free moments on the body to which they attach. High output moments can be achieved using motors with relatively limited capabilities, making them attractive for space applications like satellite attitude control [1], space manipulators [2], and astronaut mobility [3], but also for improving stability in human rehabilitation technology [4] and robotics [5]. However, their use is hampered by singularities, which can prohibit SGCMGs from exerting moments in the desired direction, and can lead to gimbal lock or excessive gimbal rates.

Each single-gimbal control moment gyroscope consists of a spinning flywheel of which the spin axis can be made to pivot about a fixed orthogonal gimbal axis. This changes the direction of the flywheel angular momentum vector, as well as the angular momentum of the body to which it is attached, in the opposite sense. The internal moment associated with this angular momentum exchange is usually much larger than the moment needed to rotate the gimbal. Nominally, away from singularities, this amplified moment is adjusted as desired by coordinating the gimbal rotation rates of several SGCMGs.

If a system with SGCMGs can be modeled accurately enough to predict future states, either offline or online, singularities are dealt with implicitly by optimizing gimbal motion to achieve a prescribed momentum trajectory [6, 7]. In unpredictable environments and low-cost applications where planning methods may not provide a satisfactory solution on time [4], the use of instantaneous (nonpredictive) gimbal steering laws remains essential. However, instantaneous methods must explicitly identify when a singularity is approached and modify the gimbal rates to mitigate the undesirable effects incurred by the singularity.

The properties of singularities and the design of gimbal steering laws to explicitly overcome tracking issues have been studied extensively. Viewed as a geometric problem, Margulies and Aubrun set out the coordinate-free theory to analyze singular directions and allowable angular momentum trajectories near singularities [8]. A survey by Kurokawa related this theory to the predominant gimbal steering laws in the literature [9].

Because the gyroscopic moment is instantaneously linearly related to the gimbal angular rates, the rates are typically computed using pseudoinverse methods, possibly augmented with so-called null motion [9]. This enables redundant SGCMG configurations to adjust gimbal rates without directly affecting the output moment in order to complete additional tasks such as singularity avoidance. Singularity problems can be partially mitigated by varying the flywheel rotation rate as well [10], but this may compromise the energy and cost savings arising from the moment amplification effect.

Well-known gimbal steering laws that nominally accomplish good tracking while applying damping near singularities include the singularity-robust (SR) steering law [11] and the singular direction avoidance (SDA) steering law [12]. They originate from robot serial manipulator control, which is mathematically similar [13]. Unlike in robot manipulators, each SGCMG independently contributes to the output moment, simplifying the singularity analysis in the configuration space [14]. Although some controllers provide accurate tracking in specific regions of the momentum space [15] and avoid some singularities, they can still become trapped if there is no singularity escape strategy.

One of the few steering laws that escapes from every singularity when properly tuned for each maneuver is the offdiagonal singularity-robust (o-DSR) steering law developed by Wie [1], which modifies the pseudoinverse to enforce escape. Other methods enhance existing steering laws by perturbing the reference moment [16, 17]. In either of these approaches, the pseudoinverse is used to both enforce escape and to damp excessive gimbal rates, presenting a tradeoff between minimizing escape time and minimizing oscillatory error moments and gimbal rates [18].

An additional limitation of many steering laws is that all singularities are characterized as properties of the SGCMG configuration alone and treated equally by the escape method. Singularities are often detected using the manipulability measure or smallest singular value, and they are sometimes classified based on the possibility of singularity escape through null motion [13]. By also considering the assigned task (tracking a moment in the reference direction), an escape method can be optimized to achieve escape in the desired direction, as well as to avoid inducing dithering signals when none are needed. For example, Yamada and Jikuya described the geometric properties of singularity escape in specific directions of the momentum space [19].

In this paper, we study the properties of singularities and the reference direction in the configuration space. We introduce a new singularity measure called the tracking index, which quantifies the ability of the system to produce the current reference moment with acceptable gimbal rates. The tracking index distinguishes singularities that prohibit moment tracking from those that do not, and anticipates singularities much sooner as compared to conventional singularity measures, making singularity avoidance methods more effective. We also propose the quantity of gimbal potential, to characterize the future ability to produce the reference moment, according to the alignment of each gimbal frame with respect to the reference direction. This generalizes and formalizes our previous method, where Berry et al. outlined a control method for a collinear configuration of two gimbals [20].

Based on these singularity measures, this paper proposes the directional singularity escape and avoidance (DSEA) steering law to address the limitations of existing laws. A generic escape and avoidance strategy is developed that uses null motion for singularity avoidance when possible while enforcing escape using a small moment error in the singular direction when necessary. Because escape is decoupled from the moment tracking task, no tradeoff is necessary between fast escape and avoiding excessive gimbal rates that cause transient errors. Instead, a task-priority mechanism is used to integrate the escape task with moment tracking, where the tracking task priority is reduced as a function of proximity to a singularity [21].

The proposed DSEA steering law results in smaller tracking errors, lower peak gimbal rates, and faster singularity escape as compared to existing methods. It is studied analytically, and its performance is demonstrated using simulations of a satellite with a pyramid configuration of four control moment gyroscopes.

Section II presents the dynamics of a satellite equipped with SGCMGs and the resulting singularity problem, for which new singularity measures are presented in Sec. III. The DSEA steering law is described in Secs. IV and V. It is evaluated and compared with [1] using simulations[a] in Sec. VI.

II. Modeling Systems with SGCMGS

A. System Model

The rigid-body dynamics of a satellite with n SGCMGs can be described using Newton–Euler equations as done by Schaub et al. [10]. The model consists of the satellite body with a body-fixed coordinate frame $\mathcal{B} : \{\hat{\boldsymbol{b}}_x, \hat{\boldsymbol{b}}_y, \hat{\boldsymbol{b}}_z\}$ and an array of n identical but arbitrarily oriented gimbal assemblies, each containing a gimbal and an axisymmetric flywheel, as shown in Fig. 1. All position vectors and inertia tensors are defined in coordinate frame $\mathcal{B}$.

Each gimbal assembly $i \in \{1, \dots, n\}$ has an associated coordinate frame $\mathcal{G}_i : \{\hat{\boldsymbol{f}}_i, \hat{\boldsymbol{g}}_i, \hat{\boldsymbol{h}}_i\}$, representing the gyroscopic moment output axis, gimbal axis, and flywheel spin axis, respectively, defined as unit vectors in $\mathcal{B}$ coordinates. Flywheel i spins about the $\hat{\boldsymbol{h}}_i$ axis with an angular rate Ω_i. The gimbal axis $\hat{\boldsymbol{g}}_i$ is fixed in $\mathcal{B}$, whereas $\hat{\boldsymbol{h}}_i(\gamma_i)$ and $\hat{\boldsymbol{f}}_i(\gamma_i)$ rotate in a plane perpendicular to $\hat{\boldsymbol{g}}_i$ by a gimbal angle γ_i:

$$\hat{\boldsymbol{h}}_i(\gamma_i) = \hat{\boldsymbol{h}}_i(0)\cos\gamma_i + \hat{\boldsymbol{f}}_i(0)\sin\gamma_i \tag{1}$$

$$\hat{\boldsymbol{f}}_i(\gamma_i) = -\hat{\boldsymbol{h}}_i(0)\sin\gamma_i + \hat{\boldsymbol{f}}_i(0)\cos\gamma_i \tag{2}$$

A positive gimbal rate $\dot{\gamma}_i$ is accompanied by a gyroscopic moment in the direction $\hat{\boldsymbol{f}}_i$ acting on the SGCMG.

The satellite body inertia tensor is $\boldsymbol{J}_B = \mathrm{diag}(J_{Bx}, J_{By}, J_{Bz})$, including the contribution of the gimbal assembly masses. The gimbal inertia is $\boldsymbol{J}_G = \mathrm{diag}(J_{Gf}, J_{Gg}, J_{Gh})$, the flywheel inertia is $\boldsymbol{J}_W = \mathrm{diag}(J_{Wf}, J_{Wg}, J_{Wh})$, and the combined inertia of a gimbal assembly is denoted $\boldsymbol{J}_T = \boldsymbol{J}_G + \boldsymbol{J}_W$. The system's total inertia matrix is

$$\boldsymbol{J}_S = \boldsymbol{J}_B + J_{Tf}\boldsymbol{F}\boldsymbol{F}^T + J_{Tg}\boldsymbol{G}\boldsymbol{G}^T + J_{Th}\boldsymbol{H}\boldsymbol{H}^T$$

[a] The MATLAB source code is available at: http://doi.org/10.4121/uuid:fe0d2307-354f-449d-b786-f063df1723c2

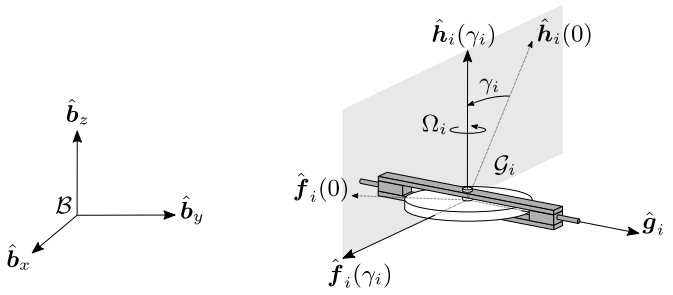

Figure 1. Frame definitions for the *i*th single-gimbal control moment gyroscope.

where $\boldsymbol{F}$, $\boldsymbol{G}$, and $\boldsymbol{H}$ are collections of gimbal frame axes:

$$\boldsymbol{F} = \begin{bmatrix} \hat{\boldsymbol{f}}_1 & \cdots & \hat{\boldsymbol{f}}_n \end{bmatrix} \tag{3}$$

$$\boldsymbol{G} = \begin{bmatrix} \hat{\boldsymbol{g}}_1 & \cdots & \hat{\boldsymbol{g}}_n \end{bmatrix} \tag{4}$$

$$\boldsymbol{H} = \begin{bmatrix} \hat{\boldsymbol{h}}_1 & \cdots & \hat{\boldsymbol{h}}_n \end{bmatrix} \tag{5}$$

For satellite attitude control, the SGCMG system is usually designed to nominally produce moments in any direction ($\mathbb{R}^3$). This paper considers SGCMG designs where the fixed $\hat{\boldsymbol{g}}_i$ are not all coplanar to minimize the worst-case tracking loss [9], called independent configurations. This class includes the well-known pyramid configuration with four SGCMGs.

The proposed singularity measures and steering law are also suited to a class of SGCMG systems that nominally produce moments in a body-fixed plane ($\mathbb{R}^2$), using a collinear configuration of gimbal axes orthogonal to that plane. By appropriately selecting the body frame $\mathcal{B}$, the matrices of Eqs. (3–5) can be adapted to remove the out-of-plane component when evaluating the controller equations. An example of a planar system for a wearable balancing assistance device was given in [4]. Both classes can be studied in terms of the task of producing a moment in $\mathbb{R}^m$ with an array of $n \geq m$ gimbals, where $m = 2$ or $m = 3$.

B. Equations of Motion

The equations of motion are obtained from [10]. Rewriting the model to use motor torques as inputs and angular accelerations as outputs gives

$$\begin{bmatrix} \dot{\boldsymbol{\omega}} \\ \ddot{\boldsymbol{\gamma}} \\ \dot{\boldsymbol{\Omega}} \end{bmatrix} = \Phi^{-1} \left(\begin{bmatrix} \boldsymbol{M}_{\text{ext}} \\ \boldsymbol{M}_g \\ \boldsymbol{M}_h \end{bmatrix} + \begin{bmatrix} -\boldsymbol{M}_\omega - \boldsymbol{\omega} \times (\boldsymbol{J}_S\, \boldsymbol{\omega}) \\ \boldsymbol{M}_\gamma \\ \boldsymbol{M}_\Omega \end{bmatrix} \right) \tag{6}$$

where the generalized mass matrix Φ is given by

$$\Phi = \begin{bmatrix} \boldsymbol{J}_S & J_{Tg}\boldsymbol{G} & J_{Wh}\boldsymbol{H} \\ J_{Tg}\boldsymbol{G}^T & J_{Tg}\boldsymbol{I}_n & \boldsymbol{0}_n \\ J_{Wh}\boldsymbol{H}^T & \boldsymbol{0}_n & J_{Wh}\boldsymbol{I}_n \end{bmatrix} \tag{7}$$

In this model, $\boldsymbol{\omega} \in \mathbb{R}^3$ is the satellite angular velocity with respect to the inertial frame expressed in $\mathcal{B}$ coordinates, $\boldsymbol{\gamma} \in \mathbb{R}^n$ contains the gimbal angles, and $\boldsymbol{\Omega} \in \mathbb{R}^n$ contains the flywheel angular rates. The inputs are the gimbal motor torques $\boldsymbol{M}_g \in \mathbb{R}^n$, the flywheel motor torques $\boldsymbol{M}_h \in \mathbb{R}^n$, and any external disturbance moment $\boldsymbol{M}_{\text{ext}} \in \mathbb{R}^3$ acting on the satellite, defined in the $\mathcal{B}$-frame. The $n \times n$ identity and zero matrices are denoted $\boldsymbol{I}_n$ and $\boldsymbol{0}_n$. The quantities $\boldsymbol{M}_\omega$, $\boldsymbol{M}_\gamma$, and $\boldsymbol{M}_\Omega$ are introduced for brevity of notation:

$$\begin{aligned} \boldsymbol{M}_\omega = {} & J_{Wh}\boldsymbol{F}\,\text{diag}\,(\boldsymbol{\Omega})\,\dot{\boldsymbol{\gamma}} \\ & + J_{Wh}\boldsymbol{F}\,\text{diag}\,(\boldsymbol{\Omega})\,\boldsymbol{G}^T\omega - J_{Wh}\boldsymbol{G}\,\text{diag}\,(\boldsymbol{\Omega})\,\boldsymbol{F}^T\boldsymbol{\omega} \\ & + (J_{Th} - J_{Tf} + J_{Tg})\boldsymbol{H}\,\text{diag}\left(\boldsymbol{F}^T\boldsymbol{\omega}\right)\dot{\boldsymbol{\gamma}} \\ & + (J_{Th} - J_{Tf} - J_{Tg})\boldsymbol{F}\,\text{diag}\left(\boldsymbol{H}^T\boldsymbol{\omega}\right)\dot{\boldsymbol{\gamma}} \end{aligned} \tag{8}$$

$$\boldsymbol{M}_\gamma = \text{diag}\left(\boldsymbol{F}^T\boldsymbol{\omega}\right)\left((J_{Th} - J_{Tf})\boldsymbol{H}^T\boldsymbol{\omega} + J_{Wh}\boldsymbol{\Omega}\right) \tag{9}$$

$$\boldsymbol{M}_\Omega = -\,J_{Wh}\,\text{diag}\left(\boldsymbol{F}^T\boldsymbol{\omega}\right)\,\dot{\boldsymbol{\gamma}} \tag{10}$$

C. Simplified Control Problem

The satellite can alter its angular velocity and attitude by exchanging angular momentum with the array of SGCMGs, which is accomplished by rotating one or more gimbals. The exchange manifests itself as an internal moment $\boldsymbol{M}_{\text{int}}$ acting on the array of SGCMGs or, equivalently, a reaction moment $-\boldsymbol{M}_{\text{int}}$ acting on the satellite body. The equations of motion for the satellite body can be obtained from (6), revealing the expression for this internal moment:

$$\begin{aligned} \boldsymbol{J}_S\,\dot{\boldsymbol{\omega}} + \boldsymbol{\omega} \times (\boldsymbol{J}_S\,\boldsymbol{\omega}) &= \boldsymbol{M}_{\text{ext}} - \boldsymbol{M}_\omega - J_{Tg}\boldsymbol{G}\ddot{\boldsymbol{\gamma}} - J_{Wh}\boldsymbol{H}\dot{\boldsymbol{\Omega}} \\ &= \boldsymbol{M}_{\text{ext}} - \boldsymbol{M}_{\text{int}} \end{aligned} \tag{11}$$

If we assume that the gimbal assembly moment of inertia $\boldsymbol{J}_T$ is small compared to the satellite body inertia $\boldsymbol{J}_B$, then $\boldsymbol{J}_S \approx \boldsymbol{J}_B$ and Eq. (11) represents the equations of motion for the satellite body subject to a moment $\boldsymbol{M}_{\text{ext}} - \boldsymbol{M}_{\text{int}}$. All flywheels rotate at a constant rate Ω_c, such that $\dot{\boldsymbol{\Omega}} = 0$. If the gimbal accelerations $\ddot{\boldsymbol{\gamma}}$ are also small, then $\boldsymbol{M}_{\text{int}} \approx \boldsymbol{M}_\omega$. Noting that $\|\boldsymbol{\omega}\| \ll \Omega_c$ further simplifies the approximation:

$$\boldsymbol{M}_{\text{int}} \approx \boldsymbol{\tau} + \boldsymbol{M}_d, \tag{12}$$

where

$$\boldsymbol{\tau} = \mu\boldsymbol{F}\dot{\boldsymbol{\gamma}} \tag{13}$$

is a gyroscopic moment that can be adjusted by choosing the gimbal rotation rate $\dot{\boldsymbol{\gamma}}$, and

$$\boldsymbol{M}_d = \mu(\boldsymbol{F}\boldsymbol{G}^T - \boldsymbol{G}\boldsymbol{F}^T)\boldsymbol{\omega} \tag{14}$$

is a disturbance gyroscopic moment due to the satellite rotation rate $\boldsymbol{\omega}$. The constant $\mu = J_{Wh}\Omega_c$ is the spin angular momentum magnitude of one flywheel. Because of the importance of the adjustable gyroscopic moment in the remainder of this paper, it is designated by the symbol $\boldsymbol{\tau}$ to distinguish it from all other moments, denoted by the letter $\boldsymbol{M}$.

The goal is to regulate the internal moment $\boldsymbol{M}_{\text{int}}$ in Eq. (12) to reproduce a reference moment $\boldsymbol{M}_{\text{int,ref}}$, in order to make the satellite complete a maneuver or reject an external disturbance. Doing so is accomplished by choosing gimbal rotation rates $\dot{\boldsymbol{\gamma}}$ that make the gyroscopic moment $\boldsymbol{\tau}$ in Eq. (13) reproduce the gyroscopic reference moment

$$\boldsymbol{\tau}_{\text{ref}} = \boldsymbol{M}_{\text{int,ref}} - \boldsymbol{M}_d \tag{15}$$

as accurately as possible. In practice, the gimbal rates cannot change instantaneously. Instead, we select commanded gimbal rates $\dot{\boldsymbol{\gamma}}_c$ and use the acceleration law

$$\ddot{\boldsymbol{\gamma}} = k_{\dot{\gamma}}\,(\dot{\boldsymbol{\gamma}}_c - \dot{\boldsymbol{\gamma}}) \tag{16}$$

to ensure that $\dot{\boldsymbol{\gamma}}$ follows $\dot{\boldsymbol{\gamma}}_c$ asymptotically [22], where $k_{\dot{\gamma}} > 0$ is a design parameter.

D. Singularity Problem

With the given simplifications, the control objective is to find the commanded rates $\dot{\boldsymbol{\gamma}}_c$ that produce an achievable output moment $\boldsymbol{\tau}_c$ as close to $\boldsymbol{\tau}_{\text{ref}}$ as possible. The output moment may be written as

$$\boldsymbol{\tau}_c = \mu\boldsymbol{F}\dot{\boldsymbol{\gamma}}_c = \mu\sum_i \hat{\boldsymbol{f}}_i\dot{\gamma}_{c,i} \tag{17}$$

where $\dot{\gamma}_{c,i}$ is the commanded rate of the ith gimbal. The total output $\boldsymbol{\tau}_c$ is a linear combination of the vectors $\hat{\boldsymbol{f}}_i(\gamma_i) \in \mathbb{R}^m$ that describe the directions in which each individual gimbal i can instantaneously produce a moment.

Nominally, the vectors $\{\hat{\boldsymbol{f}}_1, \ldots, \hat{\boldsymbol{f}}_n\}$ collectively span $\mathbb{R}^m$ (rank $\boldsymbol{F} = m$) and any moment can be produced. When the gimbals are instantaneously oriented such that the output vectors collectively span only $\mathbb{R}^{m-1}$ (rank $\boldsymbol{F} = m-1$), there is a direction $\hat{\boldsymbol{s}}$ (and $-\hat{\boldsymbol{s}}$) orthogonal to all $\hat{\boldsymbol{f}}_i$ in which no moment can be produced ($\hat{\boldsymbol{f}}_i^T \hat{\boldsymbol{s}} = 0$ for all i). Moment tracking is disrupted in this so-called singular direction $\hat{\boldsymbol{s}}$, and the system is said to encounter a singularity. For independent-type systems ($m = 3$), a singularity occurs when all $\hat{\boldsymbol{f}}_i$ lie in one plane, and $\hat{\boldsymbol{s}}$ is the vector normal to this plane. For collinear systems ($m = 2$), it occurs when all $\hat{\boldsymbol{f}}_i$ lie (anti)parallel to one another, and the singular direction is (anti)parallel to all $\hat{\boldsymbol{h}}_i$. For both types, rank$(\boldsymbol{F}) \geq m-1$.

E. Singular Value Decomposition

Another useful tool for parameterizing moment tracking performance is the singular value decomposition of the $\boldsymbol{F}$ matrix, given by [12]

$$\boldsymbol{F} = \boldsymbol{U}\boldsymbol{S}\boldsymbol{V}^T = \begin{bmatrix} \hat{\boldsymbol{u}}_1 & \cdots & \hat{\boldsymbol{u}}_m \end{bmatrix} \begin{bmatrix} \sigma_1 & & 0 & \cdots & 0 \\ & \ddots & & & \vdots \\ 0 & & \sigma_m & \cdots & 0 \end{bmatrix} \begin{bmatrix} \hat{\boldsymbol{v}}_1^T \\ \vdots \\ \hat{\boldsymbol{v}}_m^T \\ \vdots \\ \hat{\boldsymbol{v}}_n^T \end{bmatrix} \tag{18}$$

where $\hat{\boldsymbol{u}}_j \in \mathbb{R}^m$ are the left singular vectors, spanning the m-dimensional moment output space; $\hat{\boldsymbol{v}}_j \in \mathbb{R}^n$ are the right singular vectors, spanning the n-dimensional gimbal rate input space; and σ_j are the singular values, ordered such that $\sigma_1 \geq \cdots \geq \sigma_m \geq 0$. The gimbal rate vector and the resulting output moment vector may be decomposed into their singular components as

$$\dot{\boldsymbol{\gamma}}_c = \sum_{j=1}^{n} \hat{\boldsymbol{v}}_j (\hat{\boldsymbol{v}}_j^T \dot{\boldsymbol{\gamma}}_c) \tag{19}$$

$$\boldsymbol{\tau}_c = \sum_{j=1}^{m} \hat{\boldsymbol{u}}_j (\hat{\boldsymbol{u}}_j^T \boldsymbol{\tau}_c) \tag{20}$$

The singular values σ_j represent the gain between gimbal rates in the input direction $\hat{\boldsymbol{v}}_j$ and associated gyroscopic output moment in the direction $\hat{\boldsymbol{u}}_j$, such that the total output moment may be written as

$$\boldsymbol{\tau}_c = \mu \sum_{j=1}^{m} \sigma_j \hat{\boldsymbol{u}}_j (\hat{\boldsymbol{v}}_j^T \dot{\boldsymbol{\gamma}}_c) \tag{21}$$

It follows that only the gimbal rate direction vectors $\hat{\boldsymbol{v}}_j$ with $j = 1, \ldots, m$ produce an output moment. The remaining gimbal rate vectors $\hat{\boldsymbol{v}}_j$ with $j = m+1, \ldots, n$ span the null space of $\boldsymbol{F}$. Gimbal motion composed of these vectors is called null motion and does not result in any output moment $\boldsymbol{\tau}_c$.

Close to a singularity, σ_m is small, and high gimbal rates in the direction $\hat{\boldsymbol{v}}_m$ are required to produce a moment in the $\hat{\boldsymbol{u}}_m$ direction. Exactly at the singularity, $\sigma_m = 0$, at which point the vector $\hat{\boldsymbol{v}}_m$ also becomes part of the null space of $\boldsymbol{F}$, and motion in this direction ceases to produce an output moment in the $\hat{\boldsymbol{s}} = \hat{\boldsymbol{u}}_m$ direction. Because rank$(\boldsymbol{F}) \geq m-1$ for the discussed configurations, it follows that $\sigma_j > 0$ for all $j < m$. This means that only σ_m poses a threat to performance near singularities.

III. Singularity Measures

A. Configuration-Based Singularities

Usually, the proximity to a singular configuration is quantified as a property of $\boldsymbol{F}$ alone, measuring the ability to produce a moment in the $\hat{\boldsymbol{u}}_m$ direction. Common singularity measures of this type are based on the manipulability [11] or smallest singular value σ_m [12]. Normalized to equal one when σ_m reaches its maximum, the manipulability measure δ_{man} is

$$\delta_{\text{man}} = \left(\frac{m}{n}\right)^{\frac{m}{2}} \sqrt{\det(\boldsymbol{F}\boldsymbol{F}^T)} \tag{22}$$

where a value close to zero indicates that the system is close to a singular configuration. Configuration-based singularities may be further classified according to their momentum state or null-motion properties [8]. For example, configurations with all $\hat{\boldsymbol{h}}_i$ vectors maximally projected in one direction are denoted external singularities, and the remaining configurations are denoted internal singularities.

Configuration-based measures are often used to determine when to insert damping to prevent excessive gimbal rates, as well as when to insert dithering signals to escape from a singularity [1]. However, doing so is not necessary at all types of singularities, and can even degrade system performance in some cases.

B. Singularities and the Assigned Task

Instead of considering the capability of producing a moment along $\hat{\boldsymbol{u}}_m$, it is sufficient to quantify the ability to accomplish the assigned task: that is, to produce the reference moment $\boldsymbol{\tau}_{\text{ref}}$, as discussed in robotics literature [23]. It can be shown that the moment tracking error $\boldsymbol{e} = \boldsymbol{\tau}_{\text{ref}} - \boldsymbol{\tau}_c$ associated with some pseudoinverse variant # has the magnitude

$$\|\boldsymbol{e}^{\#}\| = \|\boldsymbol{\tau}_{\text{ref}} - \mu \boldsymbol{F} \dot{\boldsymbol{\gamma}}_c^{\#}\| = \|\boldsymbol{\tau}_{\text{ref}}\| \sqrt{\sum_{j=1}^{m} (1 - z_j^{\#})^2 (\hat{\boldsymbol{u}}_j^T \hat{\boldsymbol{\tau}}_{\text{ref}})^2} \tag{23}$$

where $\hat{\boldsymbol{\tau}}_{\text{ref}} = \boldsymbol{\tau}_{\text{ref}} / \|\boldsymbol{\tau}_{\text{ref}}\|$ is the reference moment unit vector and $0 \leq z_j^{\#}(\sigma_j) \leq 1$ are functions of the singular values that differ for each method. For example, in the SR inverse, $z_j^{\text{SR}} = \sigma_j^2 \left(\sigma_j^2 + \lambda\right)^{-1}$ for some damping parameter λ [11], whereas in the SDA inverse, $z_j^{\text{SDA}} = 1$ for $j < m$ and $z_m^{\text{SDA}} = \sigma_m^2 \left(\sigma_m^2 + \lambda\right)^{-1}$ [12]. Perfect tracking is possible whenever $\|\boldsymbol{e}^{\#}\| = 0$, while it is impossible when $\|\boldsymbol{e}^{\#}\| = \|\boldsymbol{\tau}_{\text{ref}}\|$.

To characterize the instantaneous ability to track a moment in the direction $\hat{\boldsymbol{\tau}}_{\text{ref}}$, we propose a new dimensionless singularity measure called the tracking index, which is defined by

$$\delta_{\text{track}} = 1 - \sqrt{\sum_{j=1}^{m} (1 - z_j)^2 (\hat{\boldsymbol{u}}_j^T \hat{\boldsymbol{\tau}}_{\text{ref}})^2} \tag{24}$$

The tracking index ranges from 0, indicating that producing $\hat{\boldsymbol{\tau}}_{\text{ref}}$ is impossible, to 1, indicating that perfect tracking is possible. The index is not defined when no reference is requested ($\boldsymbol{\tau}_{\text{ref}} = \boldsymbol{0}$), but no value is needed in this case, as will be shown later.

When applied directly for control, the functions z_j in Eq. (23) are normally chosen to minimize the moment tracking error, but we choose different z_j for the tracking index δ_{track} in Eq. (24) to allow singularities to be anticipated even when the system is still relatively far from a singular configuration. To accomplish this, we let each z_j approach zero as soon as σ_j is smaller than a predefined acceptable value σ_{acp} that facilitates tracking with acceptable gimbal rates, using

$$z_j = \frac{\sigma_j^2}{\sigma_j^2 + \kappa_j} \tag{25}$$

where

$$\kappa_j = \sigma_{\text{acp}}^2 e^{\eta(\sigma_{\text{acp}}^2 - \sigma_j^2)} \tag{26}$$

With this choice, $z_j \approx 0$ when $\sigma_j \ll \sigma_{\text{acp}}$, $z_j = 0.5$ when $\sigma_j = \sigma_{\text{acp}}$, and $z_j \approx 1$ when $\sigma_j \gg \sigma_{\text{acp}}$. The design parameter $\eta > 0$ defines the transition steepness of this sigmoidlike function in Eq. (25). The parameter σ_{acp} can be selected to obtain the desired sensitivity: a higher value results in earlier anticipation of singularities, and vice versa. Using the same z_j for all singular components j ensures that δ_{track} is smooth, even when the system reconfigures and the order of the singular components $\hat{\boldsymbol{u}}_j$ interchanges.

In addition to incorporating the reference direction in the singularity measure, the proposed tracking index is much more sensitive to singularities than conventional measures like the manipulability. The tracking index foresees singularities that prohibit tracking well before they are reached, allowing some singularities to be avoided entirely.

C. Reference-Aligned Singularities

The singularity measure δ_{man} approaches zero as σ_m approaches zero, reflecting the inability to produce a moment in the $\hat{\boldsymbol{u}}_m$ direction. This is overly conservative because the reference moment might not have a component in that direction. In contrast, the tracking index δ_{track} approaches zero only if the system is unable to produce a moment in the $\hat{\boldsymbol{\tau}}_{\text{ref}}$ direction, which occurs when, simultaneously, σ_m approaches zero and $\hat{\boldsymbol{u}}_m$ aligns with $\pm\hat{\boldsymbol{\tau}}_{\text{ref}}$. Consequently, $\delta_{\text{track}} = 0$ identifies singularities that prohibit moment tracking in the reference direction. In damped pseudoinverse methods, these singularities result in gimbal lock.

For the configurations considered in this paper, $\sigma_j > 0$ for $j < m$ and $\sigma_m \geq 0$, which ensures that $z_j > 0$ for $j < m$ and $z_m \geq 0$. Then, using Eq. (24), it follows that $\delta_{\text{track}} = 0$ if and only if $\sigma_m = 0$ and $\hat{\boldsymbol{u}}_m^T \hat{\boldsymbol{\tau}}_{\text{ref}} = \pm 1$. We can assume that $\hat{\boldsymbol{u}}_m^T \hat{\boldsymbol{\tau}}_{\text{ref}} \geq 0$, because Eq. (18) remains valid when changing the sign of both $\hat{\boldsymbol{u}}_m$ and $\hat{\boldsymbol{v}}_m$. Consequently, for the subset of singularities that satisfy $\delta_{\text{track}} = 0$ we may write

$$\delta_{\text{track}} = 0 \Rightarrow \hat{\boldsymbol{s}} = \hat{\boldsymbol{u}}_m = \hat{\boldsymbol{\tau}}_{\text{ref}} \tag{27}$$

We denote the subset of singularities with this property reference-aligned (RA) singularities. Any other singularities (satisfying $\delta_{\text{man}} = 0$ but $\delta_{\text{track}} \neq 0$) are reference-unaligned singularities. Whereas reference-aligned singularities instantaneously completely prohibit moment tracking, the reference-unaligned singularities do not, as summarized in Table 1.

The orthogonality index presented by Oh and Vadali [22] used in our previous study [20] also identified reference-aligned singularities ($\delta_{\text{track}} = 0$), but it did not unambiguously identify configurations that allowed good reference tracking ($\delta_{\text{track}} = 1$), making it less effective for the design of a steering law.

Table 1. Singularities and reference alignment

σ_m	singularity	$\lvert\hat{\boldsymbol{u}}_m^T \hat{\boldsymbol{\tau}}_{\text{ref}}\rvert$	reference-aligned	δ_{track}	instantaneous tracking
≈ 0	yes	≈ 0	no	≈ 1	yes
≈ 0	yes	≈ 1	yes	≈ 0	no
$\gg 0$	no	≈ 0	no	≈ 1	yes
$\gg 0$	no	≈ 1	yes	≈ 1	yes

D. Nearest Reference-Aligned Singularity

As the system arrives at a reference-aligned singularity during nominal operation of a pseudoinverse method, the gimbal rates must be adjusted to achieve avoidance or escape. To determine which gimbals can increase their angular momentum in the direction of the reference after escaping from their locked state, it is instructive to describe the orientation of each gimbal with respect to the reference moment [14]. Figure 2a depicts the general situation, where $\hat{\boldsymbol{\tau}}_{\text{ref}}$ may have an arbitrary orientation with respect to the $\mathcal{G}_i$ frame axes. The vector projection of $\hat{\boldsymbol{\tau}}_{\text{ref}}$ onto the plane orthogonal to $\hat{\boldsymbol{g}}_i$ is denoted $\boldsymbol{b}_i$, and the angle between $\hat{\boldsymbol{h}}_i$ and $\boldsymbol{b}_i$ is denoted $-\pi \leq \psi_i \leq \pi$. They satisfy the properties

$$\|\boldsymbol{b}_i\| = \sqrt{1 - (\hat{\boldsymbol{g}}_i^T \hat{\boldsymbol{\tau}}_{\text{ref}})^2} \tag{28}$$

$$\cos\psi_i = \frac{1}{\|\boldsymbol{b}_i\|} \hat{\boldsymbol{h}}_i^T \hat{\boldsymbol{\tau}}_{\text{ref}} \tag{29}$$

Previously, it was established that any singularity implies $\hat{\boldsymbol{f}}_i^T \hat{\boldsymbol{s}} = 0$ for all i. Combined with Eq. (27) we find a more specific result for reference-aligned singularities:

$$\delta_{\text{track}} = 0 \quad \Rightarrow \quad \hat{\boldsymbol{f}}_i^T \hat{\boldsymbol{\tau}}_{\text{ref}} = 0, \quad i \in \{1, \ldots, n\} \tag{30}$$

Consequently, when the tracking index is zero, each gimbal is either fully saturated in the direction of the reference ($\hat{\boldsymbol{h}}_i$ is maximally projected onto $\hat{\boldsymbol{\tau}}_{\text{ref}}$), as shown in Fig. 2b, or fully antisaturated ($\hat{\boldsymbol{h}}_i$ is minimally projected onto $\hat{\boldsymbol{\tau}}_{\text{ref}}$), as shown in Fig. 2c. For a system with

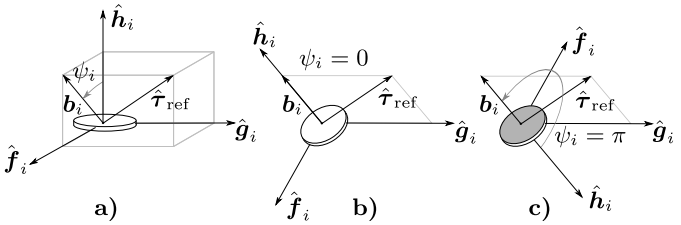

Figure 2. a) Arbitrary gimbal orientation. b) Reference-aligned saturated orientation. c) Reference-aligned anti-saturated orientation.

n SGCMGs, this leads to a total of 2^n possible singular configurations. A gimbal is closest to the fully saturated state when $|\psi_i| < \frac{1}{2}\pi$ (equivalently, $\hat{\boldsymbol{h}}_i^T \hat{\boldsymbol{\tau}}_{\text{ref}} > 0$) and closest to the fully antisaturated state when $|\psi_i| > \frac{1}{2}\pi$ (equivalently, $\hat{\boldsymbol{h}}_i^T \hat{\boldsymbol{\tau}}_{\text{ref}} < 0$). Given the current state and reference, we can express $\hat{\boldsymbol{f}}_i$ and $\hat{\boldsymbol{h}}_i$ at the nearest (anti)saturated state as

$${}^{\text{RA}}\hat{\boldsymbol{f}}_i = \begin{cases} \dfrac{\hat{\boldsymbol{g}}_i \times \hat{\boldsymbol{\tau}}_{\text{ref}}}{\|\hat{\boldsymbol{g}}_i \times \hat{\boldsymbol{\tau}}_{\text{ref}}\|} & \text{if } \hat{\boldsymbol{h}}_i^T \hat{\boldsymbol{\tau}}_{\text{ref}} > 0 \\ -\dfrac{\hat{\boldsymbol{g}}_i \times \hat{\boldsymbol{\tau}}_{\text{ref}}}{\|\hat{\boldsymbol{g}}_i \times \hat{\boldsymbol{\tau}}_{\text{ref}}\|} & \text{if } \hat{\boldsymbol{h}}_i^T \hat{\boldsymbol{\tau}}_{\text{ref}} < 0 \end{cases} \tag{31}$$

$${}^{\text{RA}}\hat{\boldsymbol{h}}_i = {}^{\text{RA}}\hat{\boldsymbol{f}}_i \times \hat{\boldsymbol{g}}_i \tag{32}$$

We define the configuration with the properties of Eqs. (31, 32) as the nearest reference-aligned singularity of the system. The left superscript RA indicates the evaluation of a system property precisely at this state. Although Eq. (31) is undefined when the reference moment is (almost) parallel to a gimbal axis ($\hat{\boldsymbol{g}}_i \times \hat{\boldsymbol{\tau}}_{\text{ref}} = \boldsymbol{0}$ and $\hat{\boldsymbol{h}}_i^T \hat{\boldsymbol{\tau}}_{\text{ref}} = 0$), it will be shown that no expressions for ${}^{\text{RA}}\hat{\boldsymbol{f}}_i$ and ${}^{\text{RA}}\hat{\boldsymbol{h}}_i$ are needed in this case.

By establishing that moment tracking is prohibited completely when $\hat{\boldsymbol{s}} = \hat{\boldsymbol{\tau}}_{\text{ref}}$, the gimbal configuration of the nearest reference-aligned singularity for the current reference $\boldsymbol{\tau}_{\text{ref}}$ can be described using Eq. (31). This prediction facilitates the design of strategies to escape from such a singular state in the desired direction, or even to avoid it entirely.

E. Gimbal Saturation and Escape Potential

At a reference-aligned singularity, all gimbals are either fully saturated or antisaturated. Whereas they are instantaneously unable to produce a moment in the reference direction, an antisaturated gimbal (see Fig. 2c) can still increase the projection of its angular momentum vector onto the reference direction, by rotating the gimbal from $|\psi_i| = \pi$ towards $\psi_i = 0$, thereby producing a moment with a component in the reference direction.

To this end, we propose the gimbal potential p_i as a per-gimbal measure for the available increase of angular momentum in the direction of the reference moment, which is defined by

$$p_i = \frac{1}{2}\|\boldsymbol{b}_i\|(1 - \cos\psi_i) = \frac{1}{2}(\|\boldsymbol{b}_i\| - \hat{\boldsymbol{h}}_i^T \hat{\boldsymbol{\tau}}_{\text{ref}}) \tag{33}$$

where the term $\frac{1}{2}(1 - \cos\psi_i)$ varies between 0 (fully saturated) and 1 (fully antisaturated). The scaling factor $0 \leq \|\boldsymbol{b}_i\| \leq 1$ accounts for the orientation of the gimbal with respect to the reference, such that gimbals that can contribute more angular momentum towards the reference direction have a correspondingly larger potential, which is in contrast to a similar saturation index proposed by Oh and Vadali [22].

The weighted sum of the gimbal potentials is a measure for the potential of the whole system to continue increasing the angular momentum in the reference direction:

$$\delta_{\text{pot}} = \frac{1}{n}\sum_{i}^{n} p_i \tag{34}$$

When $\delta_{\text{pot}} = 0$, no further increase of momentum in the reference direction is possible, meaning that the system is at a saturation singularity with respect to the reference. Some existing singularity escape

methods insert dithering signals at every singularity, regardless of the reference moment or singularity type [1]. When $\delta_{\text{pot}} = 0$, however, no escape is possible in the direction of $\hat{\boldsymbol{\tau}}_{\text{ref}}$, and escape should not be attempted in order to avoid inducing unnecessary tracking errors.

If the system is at a reference-aligned singularity where $\delta_{\text{pot}} > 0$, escaping the singularity is worthwhile, and it can be accomplished by deterministically steering antisaturated gimbals away from their antisaturated state. Because this has the effect of steering the angular momentum vectors towards the reference, the escape is said to be in the direction of the reference, even if the escape briefly leads to a small moment error in the opposite direction.

To select the gimbal rate magnitude to push it from its antisaturated state, we introduce a per-gimbal dimensionless function called the escape potential, which is defined by the following:

$$\begin{aligned} d_i &= \begin{cases} \boldsymbol{b}_i^T \boldsymbol{b}_i \cos^2 \psi_i & \text{if } \hat{\boldsymbol{h}}_i^T \hat{\boldsymbol{\tau}}_{\text{ref}} < 0 \\ 0 & \text{otherwise} \end{cases} \\ &= (\min(\hat{\boldsymbol{h}}_i^T \hat{\boldsymbol{\tau}}_{\text{ref}}, 0))^2 \end{aligned} \tag{35}$$

This expression ensures that the escape potential d_i is maximal when gimbal i is in its antisaturated state ($|\psi_i| = \pi$), and decays to zero as it approaches $|\psi_i| = \frac{1}{2}\pi$, where $\hat{\boldsymbol{h}}_i^T \hat{\boldsymbol{\tau}}_{\text{ref}} = 0$; at which point pushing the gimbal away is no longer needed. The scaling by $\boldsymbol{b}_i^T \boldsymbol{b}_i$ ensures that more effectively positioned gimbals are pushed away faster than others, allowing moment tracking to resume more quickly. Those gimbals that do not require escape can be coordinated to compensate any tracking error incurred through this operation, minimizing or even eliminating errors altogether.

To visualize the concept of deterministically pushing a gimbal from its antisaturated state, consider the pyramid arrangement of four SGCMGs [18], initially in the zero-momentum configuration of Fig. 3a, with a reference moment along the satellite body x axis. When using a pseudoinverse method, gimbals 1 and 3 would initially produce the requested moment until the system arrives at the singular configuration shown in Fig. 3b.

Although no moment can be instantaneously produced in the direction of the reference, gimbal 2 clearly has the potential to further increase the angular momentum in the direction of the reference ($p_2 > 0$), whereas the others do not ($p_1 = p_3 = p_4 = 0$). The steering law presented in the next section escapes this singularity by rotating gimbal 2 away from its antisaturated state (away from $\psi_2 = \pi$) while using the other gimbals to almost completely offset the moment error associated with doing so.

IV. Dynamic Task Allocation

A. Primary and Secondary Tasks

The primary task of the steering law is to generate gimbal rates that result in the desired gyroscopic moment $\boldsymbol{\tau}_{\text{ref}}$ whenever possible. The secondary task is to track gimbal rates $\dot{\boldsymbol{\gamma}}_s$ that provide singularity avoidance or escape while minimally impacting the primary task. Nominally, the primary task produces moments in the directions $\hat{\boldsymbol{u}}_1, \ldots, \hat{\boldsymbol{u}}_m$ using gimbal rates in the directions $\hat{\boldsymbol{v}}_1, \ldots, \hat{\boldsymbol{v}}_m$, while the secondary task employs only null motion, with gimbal rates in the directions $\hat{\boldsymbol{v}}_{m+1}, \ldots, \hat{\boldsymbol{v}}_n$.

Precisely at the singularity, the rank of $\boldsymbol{F}$ drops ($\sigma_m = 0$), and the system fails to produce a moment in the $\hat{\boldsymbol{u}}_m$ direction regardless of the gimbal rates in the $\hat{\boldsymbol{v}}_m$ direction. Consequently, the primary task loses a degree of freedom (DOF), and it is constrained to produce moments in the directions $\hat{\boldsymbol{u}}_1, \ldots, \hat{\boldsymbol{u}}_{m-1}$ using gimbal rates $\hat{\boldsymbol{v}}_1, \ldots, \hat{\boldsymbol{v}}_{m-1}$. The secondary task gains a degree of freedom, now operating with gimbal rates in the directions $\hat{\boldsymbol{v}}_m, \ldots, \hat{\boldsymbol{v}}_n$, without conflicting with the primary task.

By making the transition from nominal behavior to singular behavior smooth rather than abrupt, the secondary task can use $\hat{\boldsymbol{v}}_m$ motion: not only precisely at the singular configuration, but also close to it, which is essential to our singularity escape method. The corresponding moment in the $\hat{\boldsymbol{u}}_m$ direction only minimally affects the primary task because σ_m is very small. The dynamic transition can be accomplished optimally by selecting gimbal rates $\dot{\boldsymbol{\gamma}}_c$ that minimize the objective function given by

$$\min_{\dot{\boldsymbol{\gamma}}_c} \|\dot{\boldsymbol{\gamma}}_c - \dot{\boldsymbol{\gamma}}_s\| \quad \text{subject to} \quad \min_{\dot{\boldsymbol{\gamma}}_c} J \tag{36}$$

$$\begin{aligned} J = &(\boldsymbol{\tau}_{\text{ref}} - \mu \boldsymbol{F} \dot{\boldsymbol{\gamma}}_c)^T \boldsymbol{P} (\boldsymbol{\tau}_{\text{ref}} - \mu \boldsymbol{F} \dot{\boldsymbol{\gamma}}_c) \\ &+ (\dot{\boldsymbol{\gamma}}_s - \dot{\boldsymbol{\gamma}}_c)^T \mu^2 \boldsymbol{Q} (\dot{\boldsymbol{\gamma}}_s - \dot{\boldsymbol{\gamma}}_c) \end{aligned} \tag{37}$$

with $\boldsymbol{P} = \boldsymbol{I}_3$ and $\boldsymbol{Q} = \alpha \hat{\boldsymbol{v}}_m \hat{\boldsymbol{v}}_m^T \geq \boldsymbol{0}_n$, where α is a damping parameter.

The primary task is accomplished by minimization of the constraint cost function J, which nominally penalizes the moment tracking error $\boldsymbol{e} = \boldsymbol{\tau}_{\text{ref}} - \boldsymbol{\tau}_c$. This leads to an underdetermined set of equations, resolved by the secondary task of minimizing $\|\dot{\boldsymbol{\gamma}}_c - \dot{\boldsymbol{\gamma}}_s\|$ to make the selected gimbal rates $\dot{\boldsymbol{\gamma}}_c$ track the secondary task rates $\dot{\boldsymbol{\gamma}}_s$ as well as possible, using null motion. By letting α increase close to singularities, the primary task no longer attempts to track a moment in the $\hat{\boldsymbol{u}}_m$ direction, but instead uses gimbal rates in the $\hat{\boldsymbol{v}}_m$ direction as an additional degree of freedom for the secondary task to facilitate escape.

B. Directional Singularity Escape and Avoidance Steering Law

The optimal solution $\dot{\boldsymbol{\gamma}}_c$ that minimizes Eq. (36) is given by Chiaverini [21] as

$$\dot{\boldsymbol{\gamma}}_c = \frac{1}{\mu} \boldsymbol{F}^{\circ} \boldsymbol{\tau}_{\text{ref}} + (\boldsymbol{I}_n - \boldsymbol{F}^{\circ} \boldsymbol{F}) \dot{\boldsymbol{\gamma}}_s \tag{38}$$

where $\boldsymbol{F}^{\circ} \in \mathbb{R}^{n \times m}$ is the right pseudoinverse with numerical filtering [23]:

$$\boldsymbol{F}^{\circ} = \boldsymbol{F}^T \left(\boldsymbol{F} \boldsymbol{F}^T + \alpha \hat{\boldsymbol{u}}_m \hat{\boldsymbol{u}}_m^T \right)^{-1} \tag{39}$$

The damping parameter $\alpha \geq 0$ facilitates the dynamic transition in control behavior. When σ_m becomes smaller than $\sigma_{\min}$ (the threshold below which damping is deemed necessary to prevent excessive gimbal rates), the damping value α increases, using

$$\alpha = \sigma_{\min}^2 e^{\eta(\sigma_{\min}^2 - \sigma_m^2)} \tag{40}$$

The crucial step is then to select the secondary task rates $\dot{\boldsymbol{\gamma}}_s \in \mathbb{R}^n$ to ensure singularity escape and avoidance, which will be discussed in detail in the remainder of this paper. Owing to the strategy of selecting the secondary task rates to deal with singularities based on their properties with respect to the reference direction, we name our method the directional singularity escape and avoidance (DSEA) steering law.

When $\dot{\boldsymbol{\gamma}}_s = \boldsymbol{0}$, the DSEA steering law is equivalent to the SDA strategy [12]. That is, the proposed steering law extends SDA control with a singularity escape and avoidance method while maintaining the minimal control error properties associated with modifying only the gimbal rates corresponding to the smallest singular value.

The DSEA control error $\boldsymbol{e} = \boldsymbol{\tau}_{\text{ref}} - \boldsymbol{\tau}_c$ is exclusively in the $\hat{\boldsymbol{u}}_m$ direction, given by [21]

$$\begin{aligned} \boldsymbol{e} &= \boldsymbol{\tau}_{\text{ref}} - \mu \boldsymbol{F} \dot{\boldsymbol{\gamma}}_c \\ &= \frac{\alpha}{\sigma_m^2 + \alpha} \left(\hat{\boldsymbol{u}}_m^T \boldsymbol{\tau}_{\text{ref}} - \mu \sigma_m \hat{\boldsymbol{v}}_m^T \dot{\boldsymbol{\gamma}}_s \right) \hat{\boldsymbol{u}}_m \end{aligned} \tag{41}$$

Because the escape strategy is only active near singularities (where σ_m is small) the additional error moment to facilitate escape is small. In fact, depending on the selected secondary task rates $\dot{\boldsymbol{\gamma}}_s$, the sign of $\hat{\boldsymbol{v}}_m^T \dot{\boldsymbol{\gamma}}_s$ can be the same as the sign of $\hat{\boldsymbol{u}}_m^T \boldsymbol{\tau}_{\text{ref}}$, in which case the escape strategy even serves to decrease the error.

Because the secondary task only minimally affects the tracking task, it can be optimized separately. This avoids the tradeoff discussed in [18] where low damping was desired for fast escape while high damping was needed to prevent excessive gimbal rates and oscillatory transient errors.

C. The Changing Role of the Singular Component

The DSEA gimbal rate command $\dot{\boldsymbol{\gamma}}_c$ in Eq. (38) may be decomposed into the tracking task rates $\dot{\boldsymbol{\gamma}}_p$ and the singularity escape rates $\dot{\boldsymbol{\gamma}}_e$. To

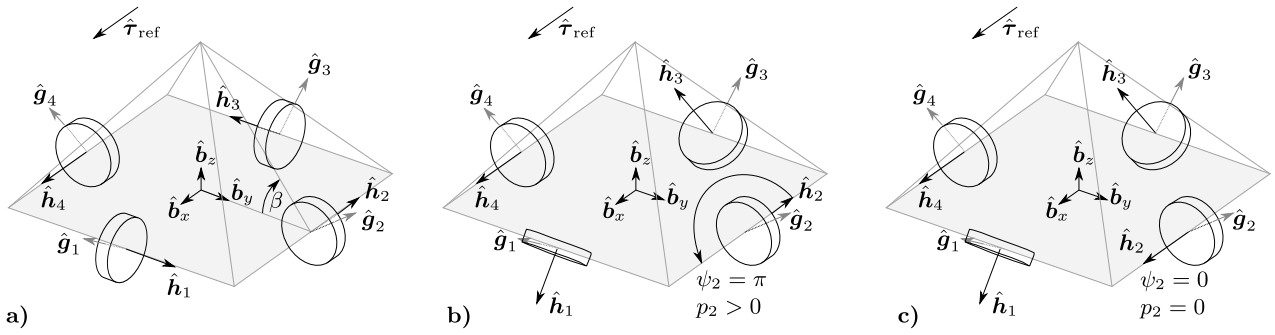

Figure 3. a) Initial gimbal configuration. b) Reference-aligned singularity with nonzero potential, indicating that tracking can resume after escape. c) Reference-aligned saturation singularity.

illustrate the controller properties, these may be further decomposed using the singular value decomposition of $\boldsymbol{F}$ as

$$\dot{\boldsymbol{\gamma}}_c = \dot{\boldsymbol{\gamma}}_p + \dot{\boldsymbol{\gamma}}_e \tag{42}$$

$$\begin{aligned}\dot{\boldsymbol{\gamma}}_p &= \frac{1}{\mu}\boldsymbol{F}^{\circ}\boldsymbol{\tau}_{\text{ref}} \\ &= \sum_{j=1}^{m-1}\frac{1}{\mu}\frac{1}{\sigma_j}\hat{\boldsymbol{v}}_j\hat{\boldsymbol{u}}_j^T\boldsymbol{\tau}_{\text{ref}} + \frac{1}{\mu}\frac{\sigma_m}{\sigma_m^2+\alpha}\hat{\boldsymbol{v}}_m\hat{\boldsymbol{u}}_m^T\boldsymbol{\tau}_{\text{ref}}\end{aligned} \tag{43}$$

$$\begin{aligned}\dot{\boldsymbol{\gamma}}_e &= (\boldsymbol{I}_n - \boldsymbol{F}^{\circ}\boldsymbol{F})\,\dot{\boldsymbol{\gamma}}_s \\ &= \underbrace{\frac{\alpha}{\sigma_m^2+\alpha}\hat{\boldsymbol{v}}_m\hat{\boldsymbol{v}}_m^T\dot{\boldsymbol{\gamma}}_s}_{\text{Additional DOF near singularities}} + \underbrace{\sum_{j=m+1}^{n}\hat{\boldsymbol{v}}_j\hat{\boldsymbol{v}}_j^T\dot{\boldsymbol{\gamma}}_s}_{\text{null motion}}\end{aligned} \tag{44}$$

The primary task gimbal rates $\dot{\boldsymbol{\gamma}}_p$ consist of a pseudoinverse solution, where the component in the direction $\hat{\boldsymbol{v}}_m$ is damped near singularities to prevent excessive gimbal rates. Because $\sigma_j > 0$ for $j < m$ and $\alpha > 0$ when $\sigma_m = 0$, the filtered pseudoinverse $\boldsymbol{F}^{\circ}$ is always well-conditioned for the considered types of SGCMG configurations.

The secondary task gimbal rates $\dot{\boldsymbol{\gamma}}_s$ are not added to the pseudoinverse solution directly, but they are filtered to obtain the actual escape rates $\dot{\boldsymbol{\gamma}}_e$ to minimize the impact on the primary task, as described by Eq. (44). The amount of filtering depends on the damping parameter α, which in turn depends on the proximity to a singularity.

Far from singularity $\alpha(\sigma_m^2+\alpha)^{-1} \approx 0$ and the $\hat{\boldsymbol{v}}_m$ component is excluded from the secondary task, resulting in pure null motion. Close to or exactly at singularity, $\alpha(\sigma_m^2+\alpha)^{-1} \approx 1$ and the $\hat{\boldsymbol{v}}_m$ component is fully included in $\dot{\boldsymbol{\gamma}}_e$, augmenting the null motion with a degree of freedom in the $\hat{\boldsymbol{v}}_m$ direction. This ensures continuity of the escape strategy in the vicinity of those singularities where the null-motion component of $\dot{\boldsymbol{\gamma}}_s$ ceases to exist.

Although the damping factor α does not take the reference direction $\hat{\boldsymbol{\tau}}_{\text{ref}}$ into account, the desired effect of activating the secondary task only near reference-aligned singularities can still be accomplished by selecting nonzero $\dot{\boldsymbol{\gamma}}_s$ only when the tracking index δ_{track} is small.

V. Selecting Secondary Task Rates

A. Role of Magnitudes and Directions

The secondary task rates $\dot{\boldsymbol{\gamma}}_s$ are designed to avoid singularities if possible, as well as to escape them with minimal moment error and escape time when needed. This is accomplished by forcing each antisaturated gimbal away from its maximally antisaturated state with respect to the reference. Cornick used a similar approach to avoid internal singularities [14], but that method could not provide escape from every singularity type due to the choice of perturbation directions and the use of null motion only [11]. In our approach, the escape magnitudes and directions are selected to provide singularity escape using motion in the null space augmented with the additional degree of freedom near singularities.

For each gimbal i, the secondary task gimbal rate magnitude $|\dot{\gamma}_{s,i}|$ is selected based on the gimbal orientation with respect to the reference direction $\hat{\boldsymbol{\tau}}_{\text{ref}}$. The direction $\theta_i \in \{-1, 0, 1\}$ is chosen to minimize the singularity escape time, so that the secondary task rate for gimbal i is $\dot{\gamma}_{s,i} = \theta_i|\dot{\gamma}_{s,i}|$. Denoting $\boldsymbol{\theta} = [\theta_1, \ldots, \theta_n]^T$ as the vector of escape directions, we get

$$\dot{\boldsymbol{\gamma}}_s(\boldsymbol{\theta}) = \begin{bmatrix}\theta_1|\dot{\gamma}_{s,1}| & \cdots & \theta_n|\dot{\gamma}_{s,n}|\end{bmatrix}^T \tag{45}$$

The magnitudes $|\dot{\gamma}_{s,i}|$ are functions of the gimbal angles and decay to zero as escape is accomplished, while the directions θ_i are selected to be locally constant during the escape.

B. Selecting Secondary Task Magnitudes

Driving an antisaturated gimbal away from its antisaturated configuration (with high escape potential d_i) when the system is near a reference-aligned singularity (with low tracking index δ_{track}) can be accomplished by making $|\dot{\gamma}_{s,i}|$ proportional to $d_i(1-\delta_{\text{track}})$:

$$\begin{aligned}|\dot{\gamma}_{s,i}| &= d_0\left\|\frac{\boldsymbol{\tau}_{\text{ref}}}{\tau_{\max}}\right\|^{\zeta}\frac{\|\boldsymbol{\tau}_{\text{ref}}\|^3}{\|\boldsymbol{\tau}_{\text{ref}}\|^3+\tau_{\min}^3}\,d_i(1-\delta_{\text{track}}) \\ &= d_0\left\|\frac{\boldsymbol{\tau}_{\text{ref}}}{\tau_{\max}}\right\|^{\zeta}\frac{1}{\|\boldsymbol{\tau}_{\text{ref}}\|^3+\tau_{\min}^3}\,\min(\hat{\boldsymbol{h}}_i^T\boldsymbol{\tau}_{\text{ref}},0)^2 \\ &\quad\cdot\sqrt{\sum_{j=1}^{m}(1-z_j)^2(\hat{\boldsymbol{u}}_j^T\boldsymbol{\tau}_{\text{ref}})^2}\end{aligned} \tag{46}$$

The regularization by $\|\boldsymbol{\tau}_{\text{ref}}\|^3(\|\boldsymbol{\tau}_{\text{ref}}\|^3+\tau_{\min}^3)^{-1}$ removes the dependency on the unit vector $\hat{\boldsymbol{\tau}}_{\text{ref}}$ in the definitions of δ_{track} and d_i, making the result unambiguous even if the reference is zero. It ensures that $|\dot{\gamma}_{s,i}| = 0$ if $\boldsymbol{\tau}_{\text{ref}} = \boldsymbol{0}$, when no escape is needed.

The design parameter $\tau_{\max}$ is the maximum moment magnitude that the system is allowed to generate, $\tau_{\min}$ is a lower limit below which moments are considered negligible, and d_0 is the maximally allowed secondary task gimbal rate. Appropriate parameters values follow from hardware specifications and a predefined maximum reference magnitude $\boldsymbol{M}_{\text{int,ref}}$ in Eq. (12). The parameter ζ sets the sensitivity of the secondary task rates to the magnitude of $\boldsymbol{\tau}_{\text{ref}}$, where a value $0 < \zeta < 1$ activates the escape strategy even for small reference moments while a larger $\zeta \geq 1$ inhibits escape until the requested moment approaches $\tau_{\max}$.

This design also ensures that $|\dot{\gamma}_{s,i}| = 0$ if $\hat{\boldsymbol{h}}_i^T\boldsymbol{\tau}_{\text{ref}} \geq 0$, so that saturated gimbals are not explicitly perturbed; rather, they are used to offset errors associated with pushing antisaturated gimbals away. At the nearest reference-aligned singularity $|\dot{\gamma}_{s,i}| = {}^{\text{RA}}|\dot{\gamma}_{s,i}|$ becomes

$${}^{\text{RA}}|\dot{\gamma}_{s,i}| = \begin{cases} d_0\left\|\dfrac{\boldsymbol{\tau}_{\text{ref}}}{\tau_{\max}}\right\|^{\zeta}\dfrac{\|\boldsymbol{\tau}_{\text{ref}}\|}{\|\boldsymbol{\tau}_{\text{ref}}\|^3+\tau_{\min}^3} & \text{if } \hat{\boldsymbol{h}}_i^T\boldsymbol{\tau}_{\text{ref}} < 0 \\ \quad\cdot\left(\boldsymbol{\tau}_{\text{ref}}^T\boldsymbol{\tau}_{\text{ref}} - (\hat{\boldsymbol{g}}_i^T\boldsymbol{\tau}_{\text{ref}})^2\right) & \\ 0 & \text{otherwise}\end{cases} \tag{47}$$

C. Selecting Secondary Task Directions

The next step in the escape and avoidance strategy is to select the secondary task directions for each gimbal that minimize the escape time and the induced escape error moment. Because $|\dot{\gamma}_{s,i}| = 0$ for gimbals satisfying $\hat{\boldsymbol{h}}_i^T \boldsymbol{\tau}_{\text{ref}} \geq 0$, we may select $\theta_i = 0$ for these gimbals without loss of generality. For the remaining n_{anti} antisaturated gimbals satisfying $\hat{\boldsymbol{h}}_i^T \boldsymbol{\tau}_{\text{ref}} < 0$, we select $\theta_i \in \{-1, 1\}$ to facilitate escape, giving $2^{n_{\text{anti}}}$ possible choices of $\boldsymbol{\theta}$.

The filtering step in Eq. (44) can change both the magnitude and direction of the secondary task rates. This has the beneficial effect of activating saturated gimbals to partially offset the errors produced by pushing the antisaturated gimbals away, but reducing the magnitudes too much can inhibit the escape. Because an antisaturated gimbal can be pushed in either direction to escape its locked state, we are free to coordinate the directions of all gimbals to minimize this inhibition. In principle, this could be done by selecting the directions $\boldsymbol{\theta}$ that minimize the difference between the selected $\dot{\boldsymbol{\gamma}}_s$ and the actually applied escape rates $\dot{\boldsymbol{\gamma}}_e$:

$$\underset{\boldsymbol{\theta}}{\operatorname{argmin}} \|\dot{\boldsymbol{\gamma}}_s(\boldsymbol{\theta}) - \dot{\boldsymbol{\gamma}}_e(\boldsymbol{\theta})\| = \underset{\boldsymbol{\theta}}{\operatorname{argmin}} \|\boldsymbol{F}^{\circ} \boldsymbol{F} \dot{\boldsymbol{\gamma}}_s(\boldsymbol{\theta})\| \tag{48}$$

Existing singularity avoidance methods that use null motion to maximize some singularity measure via steepest ascent methods can experience abrupt changes in the gimbal trajectory close to singularities, because small changes in the gimbal angles can rapidly change the gradient direction of such a measure [6].

To prevent such sudden changes in our method, the optimization in Eq. (48) should be evaluated as if the system were precisely at the nearest reference-aligned singularity. This makes the escape directions $\boldsymbol{\theta}$ local properties of the singularity, which are to be kept constant until either the singularity is escaped or $\hat{\boldsymbol{\tau}}_{\text{ref}}$ changes substantially, justifying different escape directions.

Doing so would require predicting $\boldsymbol{F}$ at the nearest reference-aligned singularity, denoted ${}^{\text{RA}}\boldsymbol{F}$. Because ${}^{\text{RA}}\hat{\boldsymbol{f}}_i$ in Eq. (31) may be undefined if $\boldsymbol{\tau}_{\text{ref}}$ happens to be parallel to a gimbal axis $\hat{\boldsymbol{g}}_i$, we slightly modify the optimization and use an objective that relies only on well-defined ${}^{\text{RA}}\hat{\boldsymbol{f}}_i$ axes. The minimization of Eq. (48) implies selecting $\boldsymbol{\theta}$ to minimize the moment-producing components in $\dot{\boldsymbol{\gamma}}_s$, because $\dot{\boldsymbol{\gamma}}_e$ is obtained by removing the moment-producing gimbal rates from $\dot{\boldsymbol{\gamma}}_s$. This is similar to choosing $\boldsymbol{\theta}$ to minimize the moment $\boldsymbol{\tau}_s$ that would be produced if $\dot{\boldsymbol{\gamma}}_s$ were applied directly, without filtering. The moment $\boldsymbol{\tau}_s$ and the modified minimization objective are written as

$$\underset{\boldsymbol{\theta}}{\operatorname{argmin}} \|\boldsymbol{\tau}_s(\boldsymbol{\theta})\|, \tag{49}$$

$$\boldsymbol{\tau}_s(\boldsymbol{\theta}) = \mu \boldsymbol{F} \dot{\boldsymbol{\gamma}}_s = \mu \sum_{i=1}^{n} \theta_i \hat{\boldsymbol{f}}_i |\dot{\gamma}_{s,i}| \tag{50}$$

Those gimbals for which ${}^{\text{RA}}\hat{\boldsymbol{f}}_i$ is undefined have the property $\hat{\boldsymbol{h}}_i^T \boldsymbol{\tau}_{\text{ref}} = 0$; from Eq. (46), $|\dot{\gamma}_{s,i}| = 0$, making the direction ${}^{\text{RA}}\hat{\boldsymbol{f}}_i$ irrelevant. Consequently, this modified optimization can be evaluated at the nearest reference-aligned singularity.

Note that, intuitively, this choice of secondary task directions exploits symmetry in the system when available, by choosing opposing directions to let the antisaturated gimbals cancel the collectively produced moment $\boldsymbol{\tau}_s$ as much as possible.

D. Algorithm to Select Optimal Secondary Task Rates

Optimizing Eq. (49) at the nearest reference-aligned singularity amounts to evaluating $\|{}^{\text{RA}}\boldsymbol{\tau}_s(\boldsymbol{\theta})\|$ for each of the allowed direction vectors $\boldsymbol{\theta}$ and selecting the option with the smallest moment. The procedure is as follows. Denote $\mathbb{I}$ as the set of antisaturated gimbals:

$$\mathbb{I} = \{i \mid \hat{\boldsymbol{h}}_i^T \boldsymbol{\tau}_{\text{ref}} < 0\} \tag{51}$$

All $2^{n_{\text{anti}}}$ possible choices of the vector $\boldsymbol{\theta}$ are obtained using $\theta_i \in \{-1, 1\}$ if $i \in \mathbb{I}$ and $\theta_i = 0$ otherwise. Evaluating all options to find the minimum may be written more formally as:

$$\widetilde{\boldsymbol{\theta}} = \underset{\boldsymbol{\theta}}{\operatorname{argmin}} \|{}^{\text{RA}}\boldsymbol{\tau}_s(\boldsymbol{\theta})\| \tag{52}$$

$${}^{\text{RA}}\boldsymbol{\tau}_s(\boldsymbol{\theta}) = \mu \sum_{\mathbb{I}} \theta_i \, {}^{\text{RA}}\hat{\boldsymbol{f}}_i \, {}^{\text{RA}}|\dot{\gamma}_{s,i}| \tag{53}$$

The steps to evaluate Eqs. (51)–(53) and obtain the optimal secondary task rates $\dot{\boldsymbol{\gamma}}_s$ are summarized in Algorithm 1. Note that for the choice $\widetilde{\boldsymbol{\theta}}$, the directions $-\widetilde{\boldsymbol{\theta}}$ produce the same $\|{}^{\text{RA}}\boldsymbol{\tau}_s\|$. Likewise, for redundant systems with multiple equally-oriented gimbals, various different $\boldsymbol{\theta}$ may produce the same optimum.

To prevent rapid switching of directions from one control time step to the next (known as chattering), we prevent a change in direction (enforce $\boldsymbol{\theta}_{t_k} = \boldsymbol{\theta}_{t_{k-1}}$) if the system is still dealing with the same reference-aligned singularity as in the previous time step (if $\mathbb{I}_{t_k} = \mathbb{I}_{t_{k-1}}$), and the change in $\|{}^{\text{RA}}\boldsymbol{\tau}_s\|$ due to switching is negligible (smaller than $\tau_{\min}$). Otherwise, if the directions must change, we choose either $\widetilde{\boldsymbol{\theta}}$ or $-\widetilde{\boldsymbol{\theta}}$: whichever leads to the smallest change in $\dot{\boldsymbol{\gamma}}_s$. The steps to obtain these piece-wise constant optimal directions $\boldsymbol{\theta}^*$ may be summarized as $\boldsymbol{\theta}^* = \text{PreventChattering}(\widetilde{\boldsymbol{\theta}})$, as described in Algorithm 2. The subscripts t_k and t_{k-1} denote the evaluation at current and previous control time step, respectively.

Algorithm 1 Selecting optimal secondary task directions

if $\mathbb{I} = \emptyset$ or $\|\boldsymbol{\tau}_{\text{ref}}\| < \tau_{\min}$ **then** ▷ Eq. (51)
  $\dot{\boldsymbol{\gamma}}_s = \boldsymbol{0}$
else
  for all $i \in \mathbb{I}$ **do**
    Evaluate ${}^{\text{RA}}\hat{\boldsymbol{f}}_i$, $|\dot{\gamma}_{s,i}|$, and ${}^{\text{RA}}|\dot{\gamma}_{s,i}|$ ▷ Eqs. (31,46,47)
  for all $2^{n_{\text{anti}}}$ possible vectors $\boldsymbol{\theta}$ **do**
    Evaluate $\|{}^{\text{RA}}\boldsymbol{\tau}_s(\boldsymbol{\theta})\|$ ▷ Eq. (52)
  From these options, take $\widetilde{\boldsymbol{\theta}} = \operatorname{argmin} \|{}^{\text{RA}}\boldsymbol{\tau}_s(\boldsymbol{\theta})\|$
  $\boldsymbol{\theta}^* = \text{PreventChattering}(\widetilde{\boldsymbol{\theta}})$ ▷ Alg. 2
  $\dot{\boldsymbol{\gamma}}_s = \dot{\boldsymbol{\gamma}}_s(\boldsymbol{\theta}^*)$ ▷ Eq. (45)

Algorithm 2 Evaluation of $\boldsymbol{\theta}^* = \text{PreventChattering}(\widetilde{\boldsymbol{\theta}})$

Denote $\Delta = \|{}^{\text{RA}}\boldsymbol{\tau}_s(\widetilde{\boldsymbol{\theta}})\| - \|{}^{\text{RA}}\boldsymbol{\tau}_s(\boldsymbol{\theta}^*_{t_{k-1}})\|$
if $\mathbb{I}_{t_k} = \mathbb{I}_{t_{k-1}}$ and $|\Delta| < \tau_{\min}$ **then**
  $\boldsymbol{\theta}^*_{t_k} = \boldsymbol{\theta}^*_{t_{k-1}}$
else
  if $\|\dot{\boldsymbol{\gamma}}_s(\widetilde{\boldsymbol{\theta}}) - \dot{\boldsymbol{\gamma}}_{s,t_{k-1}}\| < \|\dot{\boldsymbol{\gamma}}_s(\widetilde{\boldsymbol{\theta}}) + \dot{\boldsymbol{\gamma}}_{s,t_{k-1}}\|$ **then**
    $\boldsymbol{\theta}^*_{t_k} = \widetilde{\boldsymbol{\theta}}$
  else
    $\boldsymbol{\theta}^*_{t_k} = -\widetilde{\boldsymbol{\theta}}$

E. Existence of Singularity Escape Rates

Conventional null-space methods use only linear combinations of the null-space vectors $\hat{\boldsymbol{v}}_{m+1}, \ldots, \hat{\boldsymbol{v}}_n$, whereas the DSEA escape strategy can also use gimbal motion along $\hat{\boldsymbol{v}}_m$ when close to singularities. This extra degree of freedom comes with a small additional moment, yet it is crucial to ensuring singularity escape. Because the dynamically enlarged null space does not change abruptly at the singularity, any gimbal rate $\dot{\boldsymbol{\gamma}}_e$ generated exactly at the singularity continues to exist close to the singularity, thus allowing the escape to complete.

We will first demonstrate the existence of singularity escape rates $\dot{\boldsymbol{\gamma}}_e$ capable of steering gimbals out of the antisaturated state, precisely at the reference-aligned singularity, for independent-type systems ($m = 3$). Because the gimbal axes are assumed to be not all coplanar and $n \geq 3$, for any gimbal i there are at least two other gimbals k and l that are not collinear, i.e. $\hat{\boldsymbol{g}}_i \neq \pm\hat{\boldsymbol{g}}_k \neq \pm\hat{\boldsymbol{g}}_l$. Using Eq. (31), this implies ${}^{\text{RA}}\hat{\boldsymbol{f}}_i \neq \pm {}^{\text{RA}}\hat{\boldsymbol{f}}_k \neq \pm {}^{\text{RA}}\hat{\boldsymbol{f}}_l$, yet Eq. (30) shows that they all lie in the same plane orthogonal to $\hat{\boldsymbol{\tau}}_{\text{ref}}$, making them linearly dependent. That is, any ${}^{\text{RA}}\hat{\boldsymbol{f}}_i$ can be written as some linear combination of ${}^{\text{RA}}\hat{\boldsymbol{f}}_k$ and ${}^{\text{RA}}\hat{\boldsymbol{f}}_l$.

Therefore, the effect of a secondary task gimbal rate involving gimbal i can be canceled using motion with gimbals k and l. In other words, at the state of reference-aligned singularity there exists null motion that can rotate any gimbal i, so that selecting nonzero $\dot{\gamma}_{s,i}$ results in nonzero $\dot{\gamma}_{e,i}$. In fact, the procedure in Eq. (52) implicitly selects the direction vector $\boldsymbol{\theta}$ that maximizes null motion, by minimizing the difference beteen $\dot{\boldsymbol{\gamma}}_e$ and $\dot{\boldsymbol{\gamma}}_s$.

Because of continuity and the locally constant escape directions, gimbals are driven out of the singular configuration and towards the

reference until σ_m is no longer small: at this point the singularity is escaped and the pseudoinverse component $\dot{\boldsymbol{\gamma}}_p$ in Eq. (42) takes over.

For collinear gimbal configurations for planar applications ($m = 2$), a reference-aligned singularity implies that all $\hat{\boldsymbol{f}}_i$ are collinear and orthogonal to $\hat{\boldsymbol{\tau}}_{\text{ref}}$. Since $n \geq 2$, for any gimbal i there is another gimbal k that can cancel its moment exactly, meaning that null motion exists exactly at the reference-aligned singularity. Escape rates continue to exist beyond the singularity, following the same argument as previously stated.

VI. Controller Evaluation

A. Simulation Properties

The simulation model comprises a satellite equipped with $n = 4$ SGCMGs positioned in a pyramid configuration with skew angle β, as shown in Fig. 3. The gimbal axes and the angular momentum axes for $\gamma_i = 0$ are given by

$$\boldsymbol{G} = \begin{bmatrix} \sin\beta & 0 & -\sin\beta & 0 \\ 0 & \sin\beta & 0 & -\sin\beta \\ \cos\beta & \cos\beta & \cos\beta & \cos\beta \end{bmatrix} \tag{54}$$

$$\boldsymbol{H}(\boldsymbol{0}) = \begin{bmatrix} 0 & -1 & 0 & 1 \\ 1 & 0 & -1 & 0 \\ 0 & 0 & 0 & 0 \end{bmatrix} \tag{55}$$

The transverse axes for $\gamma_i = 0$ follow using $\hat{\boldsymbol{f}}_i(0) = \hat{\boldsymbol{g}}_i \times \hat{\boldsymbol{h}}_i(0)$ and the axes orientations for arbitrary γ_i are obtained using Eq. (1). The satellite model parameters are listed in Table 2. The values are based on [18], but the inertia parameters are decreased by two orders of magnitude, reflecting more recent developments of smaller satellites. Note that because the controller requires only $n \geq m$ with non-coplanar gimbal axes, it is still applicable if one gyroscope fails, as long as control parameters are adapted accordingly.

With $n = 4$ and $m = 3$, the satellite nominally produces moments in any direction (primary task), and the avoidance strategy nominally operates using only null-motion component $\hat{\boldsymbol{v}}_4$ (secondary task). Near a singularity, the primary task output reduces to a plane, where any moment is produced using motion in the $\hat{\boldsymbol{v}}_1$ and $\hat{\boldsymbol{v}}_2$ directions, while the secondary task uses $\hat{\boldsymbol{v}}_3$ and $\hat{\boldsymbol{v}}_4$ to provide singularity escape, with a small moment in the $\hat{\boldsymbol{u}}_3$ direction.

Table 2. Model parameters

Symbol	Value	Units	Symbol	Value	Units
n	4	-	μ	10	Nm · s
m	3	-	Ω_c	500	rad/s
β	$\cos^{-1} 0.6$	rad	$k_{\dot{\gamma}}$	40	s^{-1}
J_{Wh}	0.02	kg · m^2	k_Ω	10^{-5}	s^{-1}
J_{Tf};J_{Tg};J_{Th}	0.01; 0.01; 0.02	kg · m^2	k_p	7	s^{-2}
J_{Bx};J_{By};J_{Bz}	214; 201; 50	kg · m^2	k_v	3	s^{-1}

The gimbal steering law is evaluated at a frequency of $\nu = 100$ Hz. At each time step, the gimbal rate command $\dot{\boldsymbol{\gamma}}_c$ is obtained using the steering law in Eq. (38), for which the secondary rates $\dot{\boldsymbol{\gamma}}_s$ are obtained using Algorithms 1 and 2. The necessary gimbal accelerations given by Eq. (16) can be obtained using the gimbal and flywheel motor torques [10, 22]

$$\boldsymbol{M}_g = k_{\dot{\gamma}} \left(\dot{\boldsymbol{\gamma}}_c - \dot{\boldsymbol{\gamma}}\right) J_{Tg} \quad + J_{Tg} \boldsymbol{G}^T \dot{\boldsymbol{\omega}}_c \; - \boldsymbol{M}_\gamma \tag{56}$$

$$\boldsymbol{M}_h = k_\Omega \left(\boldsymbol{\Omega}_c - \boldsymbol{\Omega}\right) J_{Wh} + J_{Wh} \boldsymbol{H}^T \dot{\boldsymbol{\omega}}_c - \boldsymbol{M}_\Omega, \tag{57}$$

where $\boldsymbol{\Omega}_c$ is the constant vector of commanded flywheel rates (Ω_c for each flywheel), the control gains $k_{\dot{\gamma}}$ and k_Ω specify the motor torques for deviations from the commanded motor speeds, and $\dot{\boldsymbol{\omega}}_c$ is the instantaneous satellite body angular acceleration obtained from (11) given the imposed gimbal and flywheel accelerations:

$$\begin{aligned} \dot{\boldsymbol{\omega}}_c = \boldsymbol{J}_S^{-1} \left(\boldsymbol{M}_{\text{ext}} - \boldsymbol{M}_\omega - \boldsymbol{\omega} \times (\boldsymbol{J}_S\, \boldsymbol{\omega})\right) \\ - k_{\dot{\gamma}} J_{Tg} \boldsymbol{J}_S^{-1} \boldsymbol{G} \left(\dot{\boldsymbol{\gamma}}_c - \dot{\boldsymbol{\gamma}}\right) \\ - k_\Omega J_{Wh} \boldsymbol{J}_S^{-1} \boldsymbol{H} \left(\boldsymbol{\Omega}_c - \boldsymbol{\Omega}\right) \end{aligned} \tag{58}$$

The gimbal speed controller in Eqs. (56-58) runs in continuous time. Although various simplifications were introduced in Section C for the purpose of controller design, the full dynamical model of Eq. (6) is used in these simulations. Modified Rodrigues Parameters (denoted $\boldsymbol{\rho}$) and their shadow counterparts [10] are used for the satellite kinematics. The equations of motion are integrated using a Runge-Kutta 4 algorithm with a fixed 1 ms time step.

For all simulations, the gimbals are initially at rest [$\dot{\boldsymbol{\gamma}}(t_0) = \boldsymbol{0}$] and the satellite orientation is initially zero [$\boldsymbol{\rho}(t_0) = \boldsymbol{0}$]. The initial angular velocity of the satellite is such that given the initial gimbal angles, the overall momentum in the system equals $\boldsymbol{0}$, giving

$$\boldsymbol{\omega}(t_0) = -\mu \boldsymbol{J}_S^{-1}(t_0) \boldsymbol{H}(t_0) \boldsymbol{\Omega}(t_0) \tag{59}$$

In the following simulations, moments are presented in terms of the internal moment $\boldsymbol{M}_{\text{int}}$, rather than $\boldsymbol{\tau}$. The difference is given in Eq. (15), but because of the comparatively low rotation rate of the satellite (up to 10 deg/s) it follows that $\boldsymbol{\tau}_{\text{ref}} \approx \boldsymbol{M}_{\text{int,ref}}$. This is not a requirement for using this control law, but it simplifies interpretation of the graphs.

B. Control Parameter Selection

The DSEA steering law parameters are given in Table 3, with $\tau_{\min}$, $\tau_{\max}$, d_0 and ζ selected as discussed in Section V. One can choose $\sigma_{\min}$ to limit the gimbal rates, by specifying an upper bound on the magnitude of the pseudoinverse component of the steering law. The highest pseudoinverse gimbal rates $\dot{\boldsymbol{\gamma}}_p$ [Eq. (43)] occur when $\boldsymbol{\tau}_{\text{ref}} = \tau_{\max} \hat{\boldsymbol{u}}_m$. Denoting $\dot{\gamma}_{\max}$ as the maximally allowed value of $\|\dot{\boldsymbol{\gamma}}_p\|$, we can use Eq. (21) to obtain $\sigma_{\min} = \tau_{\max}/(\mu \dot{\gamma}_{\max})$. This conservatively limits the pseudoinverse component per gimbal because $|\dot{\gamma}_{p,i}| \leq \|\dot{\boldsymbol{\gamma}}_p\| \leq \dot{\gamma}_{\max}$. After testing this initial choice of $\sigma_{\min}$, a higher value may be used to further limit the gimbal rates if necessary, and vice versa. The escape strategy may result in an additional gimbal rate of up to d_0 such that, in principle, each gimbal rate is limited by $|\dot{\gamma}_i| \leq \dot{\gamma}_{\max} + d_0$, although the gimbal rates are generally much lower.

The parameter σ_{acp} used in the tracking index δ_{track} in Eq. (25) is selected as $\sigma_{\text{acp}} > \sigma_{\min}$ in order to anticipate singularities early on, before any damping is applied. This allows the secondary task to begin operating with null motion even while far from singularities, avoiding some internal singularities.

C. o-DSR control

To enable easy comparison with the o-DSR controller proposed by Wie [1], all simulations are repeated with the gimbal steering law of Eq. (38) replaced by

$$\dot{\boldsymbol{\gamma}}_c^{\text{oDSR}} = \frac{1}{\mu} \boldsymbol{Q}^{-1} \boldsymbol{F}^T \left(\boldsymbol{F} \boldsymbol{Q}^{-1} \boldsymbol{F}^T + \boldsymbol{P}^{-1}\right)^{-1} \boldsymbol{\tau}_{\text{ref}} \tag{60}$$

$$\boldsymbol{P}^{-1} = \lambda \begin{bmatrix} 1 & \epsilon_3 & \epsilon_2 \\ \epsilon_3 & 1 & \epsilon_1 \\ \epsilon_2 & \epsilon_1 & 1 \end{bmatrix}, \quad \boldsymbol{Q}^{-1} = \begin{bmatrix} W_1 & \lambda & \lambda & \lambda \\ \lambda & W_2 & \lambda & \lambda \\ \lambda & \lambda & W_3 & \lambda \\ \lambda & \lambda & \lambda & W_4 \end{bmatrix} \tag{61}$$

$$\lambda = \lambda_1 \exp(-\lambda_2 \det(\boldsymbol{F}\boldsymbol{F}^T)) \tag{62}$$

$$\epsilon_j = \epsilon_0 \sin(\phi_0 t + \phi_j) \tag{63}$$

with the control parameters listed in Table 3. The parameters W_i can be used to adjust the amount of damping applied to each gimbal i. As discussed in [24], preceding [1], these values are selected by trial and error for each maneuver. Because the required damping for each gimbal varies with its orientation with respect to the reference signal (see

Section E), selecting suitable W_i values depends on both the maneuver direction and the gimbal angles before starting a maneuver. This makes the o-DSR method difficult to use in general, except for maneuvers known in advance, which are tuned and tested to ensure feasibility.

To analyze the effect of the offdiagonal elements ϵ_j and λ, first denote the pseudoinverse component $\dot{\boldsymbol{\gamma}}_p^{\text{oDSR}}$ as in Eq. (60), but use $\boldsymbol{P}^{-1} = \lambda \boldsymbol{I}_3$ and $\boldsymbol{Q}^{-1} = \text{diag}\{W_1, W_2, W_3, W_4\}$. The remainder $\dot{\boldsymbol{\gamma}}_e^{\text{oDSR}} = \dot{\boldsymbol{\gamma}}_c^{\text{oDSR}} - \dot{\boldsymbol{\gamma}}_p^{\text{oDSR}}$ are the gimbal rate variations that enforce singularity escape, which may be used for comparison with the $\dot{\boldsymbol{\gamma}}_e$ component of the DSEA steering law. Simulations show that $\dot{\boldsymbol{\gamma}}_e^{\text{oDSR}}$ is sinusoidal in nature. If the singularity is not escaped within half of its period, the gimbals reverse and return to the singular configuration, considerably delaying escape. The o-DSR controller escape time can be decreased by increasing the offdiagonal elements or decreasing damping, at the cost of higher transient errors and oscillations in the moment output: a tradeoff discussed in [18].

Table 3. DSEA and o-DSR control parameters

DSEA	Value	Units	o-DSR	Value	Units
σ_{acp}	0.75	-	λ_1	0.01	-
σ_{min}	0.25	-	λ_2	10	-
η	10	-	ϕ_0	$\pi/2$	rad/s
d_0	3	rad/s	ϕ_j	0; $\pi/2$; π	rad
τ_{min}	0.001	Nm	ϵ_0	0.01	-
τ_{max}	10	Nm			
ζ	0.5	-			

D. Distinguishing Singularities

Figure 4 demonstrates the DSEA controller response to the constant internal moment reference signal $\boldsymbol{M}_{\text{int,ref}} = [7.07\ \ 7.07\ \ 0]^T$ Nm when the system starts in the zero-momentum configuration of Fig. 3a. After accelerating the gimbals towards the commanded rates, the reference is tracked accurately (see Fig. 4a). A singularity is encountered at $t = 1.6$ s, as indicated by the manipulability measure δ_{man} approaching zero (Fig. 4b). However, because the tracking index is high ($\delta_{\text{track}} = 1$), the controller continues to track the reference without relying on the escape and avoidance strategy or perturbations.

Beyond $t = 3$ s, the system begins to approach another singularity. While δ_{man} is still near its peak value, δ_{track} is already approaching 0, anticipating a reference-aligned singularity. As indicated by $\delta_{\text{pot}} = 0$, this is a saturation singularity in the reference direction. Because there is no escape possible outwards from the external singular surface, the pseudoinverse solution is damped and the escape strategy is inactive in order to avoid inducing perturbations.

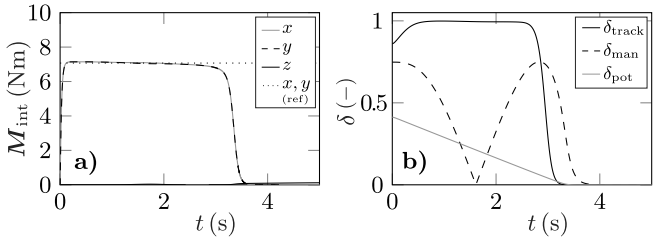

Figure 4. Identification of singularity properties allows continued tracking without explicitly inducing errors near reference-unaligned singularities.

E. Singularity Escape Performance for DSEA

The simulation in Fig. 5a–f demonstrates DSEA performance for the constant reference signal $\boldsymbol{M}_{\text{int,ref}} = [10\ \ 0\ \ 0]^T$ Nm when the system starts in the zero-momentum configuration of Fig. 3a. After tracking the reference moment for approximately one second, the system approaches the well-known singularity with $\gamma_1 = -\frac{\pi}{2}$, $\gamma_2 = 0$, $\gamma_3 = \frac{\pi}{2}$, $\gamma_4 = 0$, pictured in Fig. 3b. Because gimbal 2 is antisaturated with respect to the reference, its gimbal potential is high and a nonzero secondary task rate $\dot{\gamma}_{s,2}$ is selected (see Fig. 5d), for which the magnitude increases as the singularity approaches.

Although the secondary task activates some null motion before $t = 1$ s, this is initially insufficient to avoid the singularity. As the singularity is approached further, the secondary task becomes able to steer gimbal 2 as desired in order to escape the singularity. As shown in Figs. 5c and 5f, this causes gimbal 4 to move in order to partially cancel the induced moment. This is accomplished using motion in the $-\hat{\boldsymbol{v}}_m$ direction during $t = 1$–1.5 s and in the $\hat{\boldsymbol{v}}_m$ direction during $t = 1.5$–2 s (see Fig. 5e), thus producing small moments in the $-\hat{\boldsymbol{u}}_m$ and $\hat{\boldsymbol{u}}_m$ directions, respectively.

Because of the well-damped pseudoinverse and the consistent output of the secondary task, the escape is accomplished quickly, with limited peak gimbal rates and without any oscillations. Finally, the controller continues tracking the reference until saturation is reached: at this point the output is fully damped.

F. Singularity Escape Performance for o-DSR

Fig. 5g–i shows the results for the same simulation with the o-DSR controller. The weights W_i are tuned to increase damping of gimbal 1 [1], by choosing $W_1 = 10^{-3}$ and $W_2 = W_3 = W_4 = 0.1$. This causes gimbals 1 and 3 to attain different rates, preventing gimbals 2 and 4 from locking up, thus skewing the singularity for this particular maneuver. After briefly tracking the reference moment, gimbals 2 and 4 suddenly reverse at $t = 0.4$ s, inducing high gimbal rates and oscillations in the output moment, after which moment tracking resumes until the singularity at $t = 1$ s. It is escaped after one second, and moment tracking continues until reaching the saturation singularity at $t = 4$ s. Though no escape is is possible, the gimbals continue to be perturbed, leading to small but persistent oscillatory moment errors. This is not shown in [1], where the results after $t = 4$ s are truncated.

The gimbal rate oscillations in the o-DSR simulation in Fig. 5g–i (and Fig. 6g–i) are likely due to insufficient damping of the pseudoinverse combined with the nonzero inertia of the gimbal assemblies, the finite controller sampling rate, and the actual gimbal rates $\dot{\boldsymbol{\gamma}}$ slightly lagging the commanded rates $\dot{\boldsymbol{\gamma}}_c$ due to (16). Although these phenomena are ignored in some literature by assuming that gimbal dynamics are negligible, the oscillations may have a considerable impact on performance and durability. This type of oscillation does not occur in the DSEA controller because damping is not sacrificed to expedite singularity escape.

Damping in the o-DSR controller is further limited because the proximity to a singularity around $t = 0.4$ s goes almost unnoticed ($\delta_{\text{man}} > 0.6$), with the manipulability returning to its initial value around $t = 0.8$ s (see Fig. 5h). By comparison, the tracking index distinguishes the situation at $t = 0.4$—0.8 s from the one at $t = 0$ s, thus identifying the tracking problem.

It is also worth noting that using the same W_i parameters for a y-axis maneuver ($\boldsymbol{M}_{\text{int,ref}} = [0\ \ 10\ \ 0]^T$ Nm) causes the o-DSR controller to remain stuck in a singularity for over 6 seconds, highlighting the sensitivity to the tuning parameters. By contrast, DSEA control performance is identical for a y-axis maneuver, because the secondary task rates are automatically adjusted to the changing reference signal and gimbal angles.

G. Singularity Avoidance Performance

The simulation in Fig. 6a–f demonstrates the DSEA control performance for the constant reference signal $\boldsymbol{M}_{\text{int,ref}} = [-10\ \ 0\ \ 0]^T$ Nm when the system starts in the external singularity depicted in Fig. 3c, where $\gamma_1(t_0) = -\frac{\pi}{2}$, $\gamma_2(t_0) = \pi$, $\gamma_3(t_0) = \frac{\pi}{2}$, and $\gamma_4(t_0) = 0$ rad, as reached at the end of the previous simulation. The angular acceleration and deceleration in these simulations highlight typical elements of a satellite maneuver. The system begins in a reference-aligned singularity ($\delta_{\text{track}} = 0$ and $\delta_{\text{man}} = 0$), but the nonzero potential ($\delta_{\text{pot}} > 0$) indicates that escape in the reference direction is possible. All gimbals

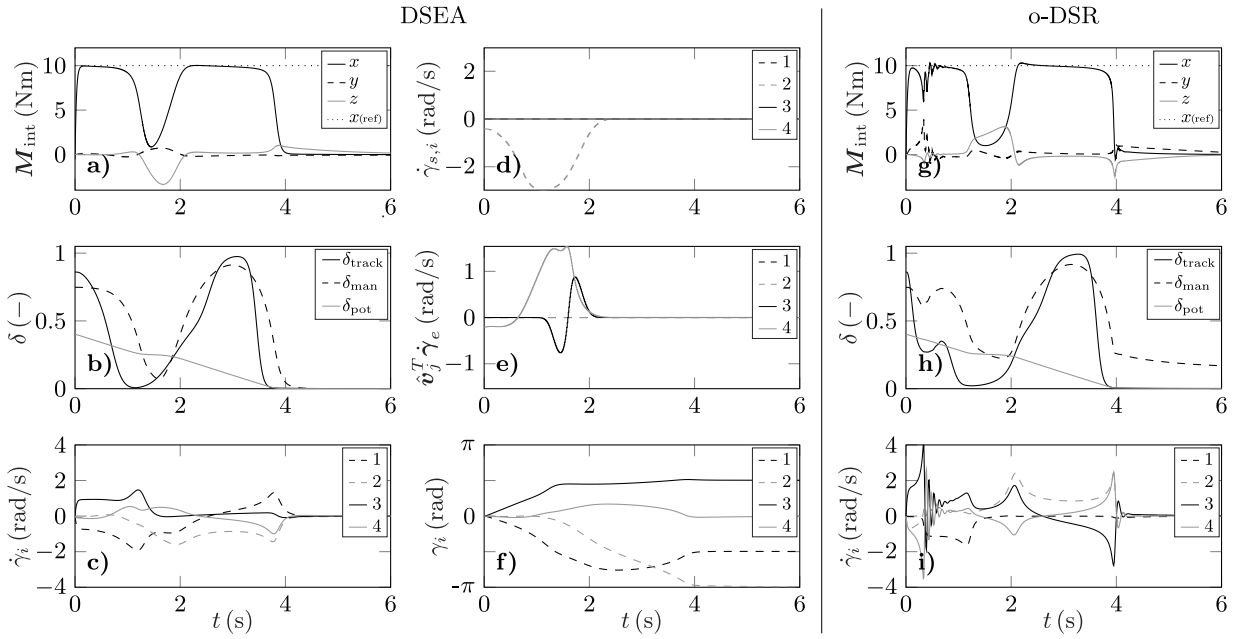

Figure 5. Early singularity anticipation and constant escape directions provide singularity escape with lower peak gimbal rates and without oscillations.

are initially π rad away from saturation in the reference direction, so that $|\dot{\gamma}_{s,i}| > 0$ (see Fig. 6d).

Null motion is unsuitable for escaping this saturation singularity, so Algorithm 1 selects the directions $\theta_2 = \theta_4 = 1$ and $\theta_1 = \theta_3 = -1$ to steer all gimbals symmetrically away from the antialigned state, achieving motion in the positive $\hat{\boldsymbol{v}}_m$ direction. The singularity is escaped and the error is reduced, because the escape moment $\mu\sigma_3\hat{\boldsymbol{u}}_3\,\hat{\boldsymbol{v}}_3^T\dot{\boldsymbol{\gamma}}_s$ is in the direction $\hat{\boldsymbol{u}}_3 = \hat{\boldsymbol{\tau}}_{\text{ref}}$. The initial overshoot of the reference moment in Figs. 6a and 6g is attributable to the slight lag of $\dot{\boldsymbol{\gamma}}$ relative to the commanded rates $\dot{\boldsymbol{\gamma}}_c$.

After escaping the singularity at $t = 0$ s, the satellite tracks the reference until it approaches an internal reference-aligned singularity around $t = 3$ s (the tracking index δ_{track} becomes small), causing the escape strategy to activate. Still being quite far from the singularity, only the null-motion component $\hat{\boldsymbol{v}}_4$ motion is available. As shown in Figs. 6c–e, the directions $\theta_1 = 1$ and $\theta_3 = -1$ result in null motion that causes the pairs of opposite gimbals 1&3 and 2&4, which are initially moving at the same rate, to attain different rates. This steers gimbals 1 and 3 away from their antisaturated states, ultimately avoiding the singularity at $t = 4$ s. After transferring all angular momentum to the satellite body, a saturation singularity is reached, at which point all gimbals are damped and the escape strategy deactivates.

In contrast, the o-DSR controller in Figs. 6g–i requires 0.2 s to initiate the escape from the initial singularity. The internal singularity at 4.3 s is not detected until it is fully encountered, leading to high gimbal rates and moment errors to escape it. High oscillatory gimbal rates are observed as the system settles in the final saturation singularity.

In this case, the o-DSR controller uses $W_i = 1$ for all gimbals. While tuning can improve performance at the internal singularity near $t = 4$ s, we found that doing so considerably delays the initial external singularity escape, and vice versa. This is because different gimbals must be damped at both singularities encountered in this simulation.

H. Performance of Attitude Control with Disturbance Rejection

This section demonstrates a pointing task while rejecting a small disturbance. As noted in the survey by Kurokawa [9], few papers have addressed this problem in detail. For simplicity, we use the reference moment generator [10] given by

$$\boldsymbol{M}_{\text{int,ref}} = \boldsymbol{J}_B\left(k_p\boldsymbol{\rho} + k_v\boldsymbol{\omega}\right) + \boldsymbol{M}_{\text{ext}} \tag{64}$$

where $\boldsymbol{\rho}$ are the Modified Rodrigues Parameters representing the satellite body attitude, k_p and k_v are proportionality and damping constants, and $\boldsymbol{M}_{\text{ext}}$ is a known disturbance.

The simulation in Fig. 7 demonstrates station-keeping performance when the system is subject to a constant disturbance of $\boldsymbol{M}_{\text{ext}} = [0.5\ \ 0\ \ 0]^T$ Nm: again starting in the zero-momentum configuration of Fig. 3a. This amounts to steering the gimbals to continuously produce a moment in the direction $[1\ \ 0\ \ 0]^T$, with a small additional component to stabilize the satellite when necessary, as shown in Fig. 7a. The error magnitude $|\boldsymbol{\rho}|$ in Figs. 7d and 7j represents the principal angle deviation from station keeping, in degrees. Note that the y axes use different scales.

The disturbance causes the system to eventually encounter the same singularity as in Fig. 3b, though at a much slower rate. This gives the avoidance strategy more time to steer gimbal 2 away from its antisaturated state almost entirely using null-motion component $\hat{\boldsymbol{v}}_4$ (see Fig. 7e). Ultimately, some $\hat{\boldsymbol{v}}_3$ motion with a small moment error is needed to complete the escape just as the simulation of Fig. 5, but tracking is almost uninterrupted, leading to only a minor deviation in the satellite attitude.

Figures 7b and 7h demonstrate the effectiveness of the tracking index δ_{track}, anticipating the singularity much sooner than the manipulability measure δ_{man}. Because the o-DSR controller relies on δ_{man}, its escape strategy is inactive until the singularity is fully encountered around $t = 24$ s, at which point tracking is severely hampered.

Because the reference moment is initially small, the intrinsic perturbations of the o-DSR method are too small to result in singularity escape. The reference moment magnitude ultimately grows along with the increasing attitude error until escape is accomplished. The associated attitude error of the o-DSR controller is more than 50 times as high as with the DSEA controller, and higher gimbal rates are necessary for the escape. Though $W_i = 1$ is used here for all gimbals, we found that choosing other values does not substantially improve escape time because of the equally delayed singularity detection.

VII. Conclusion and Discussion

The tracking index and gimbal potential represent new contributions to solving the singularity problem of single-gimbal control moment gyroscopes. These singularity measures distinguish singularities that prohibit moment tracking from those that do not, and they exploit the alignment of the reference moment and the singular direction to predict the gimbal configuration at the nearest singularity.

Based on these properties, a directional singularity escape and avoidance steering law has been designed that minimizes escape time and the moment tracking error, with limited peak gimbal rates, using

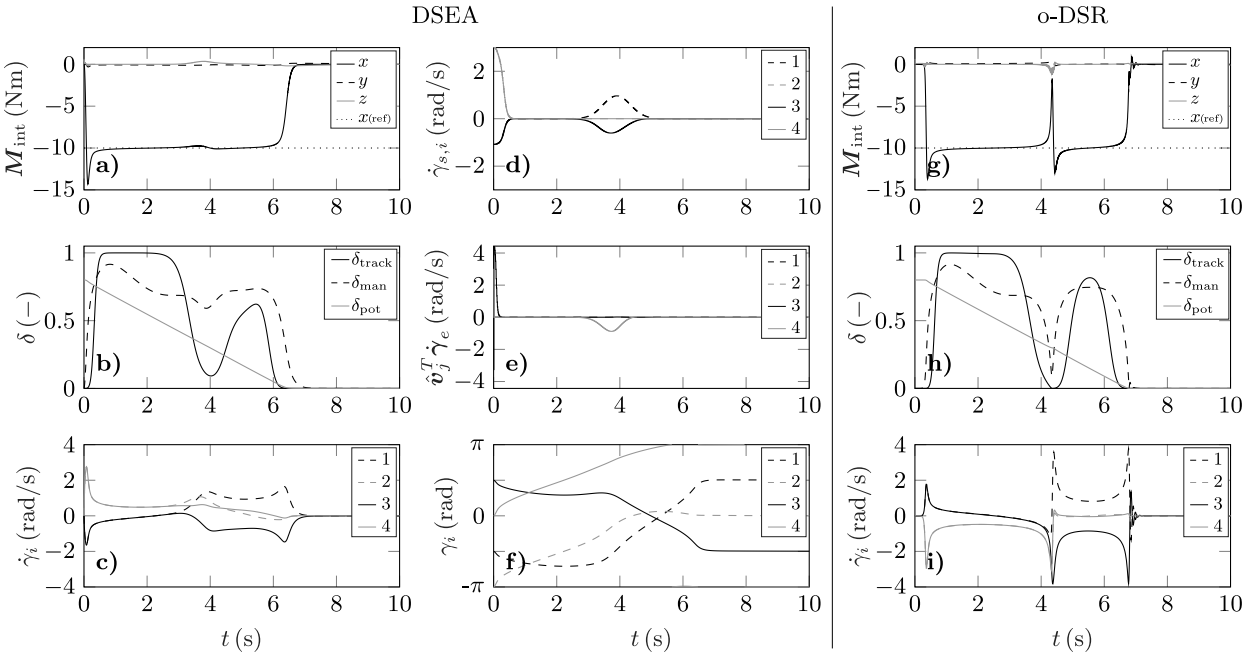

Figure 6. The secondary task symmetrically steers opposite gimbals apart to escape and avoid two singularities.

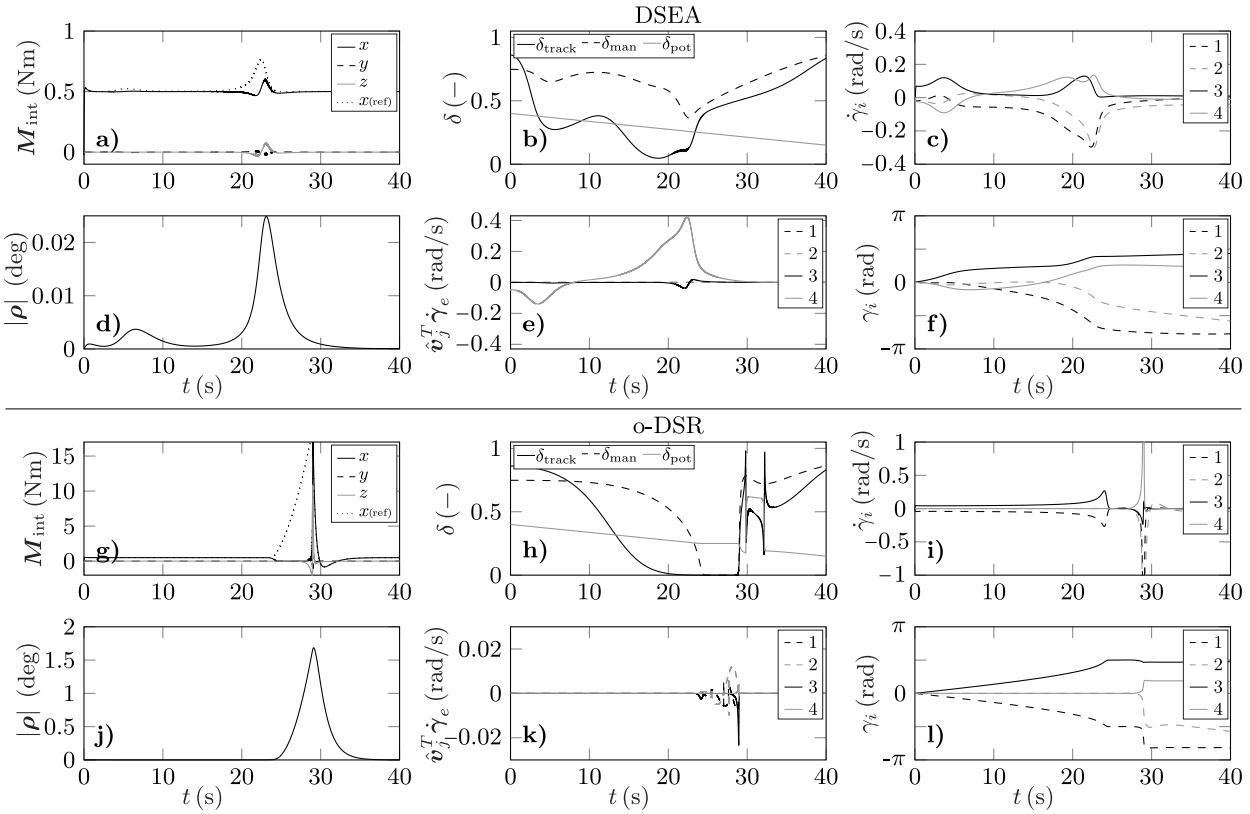

Figure 7. Disturbance rejection during station keeping. The secondary task avoids the internal singularity almost entirely using null motion.

null motion whenever possible. By dynamically giving the escape strategy an additional degree of freedom close to singularities, fast escape can be enforced if requested, as shown analytically and as demonstrated using simulations.

Compared to existing instantaneous gimbal steering laws, which merge the moment tracking and singularity escape objectives by perturbing the system at every type of singularity, the presented steering law operates with less moment error, less delay in singularity escape, and lower peak gimbal rates, without tuning the controller separately for each maneuver. Instead, the presented method exploits the whole momentum space and efficiently deals with all types of singularities, using a single set of control parameters that can be selected based on physical and intuitive considerations.

The analytical study of the existence of singularity escape gimbal rates provides stronger support for singularity escape in the reference direction than guaranteeing nonzero gimbal rates, as done in most existing literature. However, although simulations have yet to disprove our method, further research is needed to devise a formal proof.

Further confidence in the effectiveness of the DSEA method may be obtained using simulations to validate singularity escape for a wide variety of reference moment directions on the unit sphere and initial gimbal angles along a full rotation, up to a desired level of accuracy. Similar benchmarks may be used to evaluate rest-to-rest maneuvers or to analyze new gimbal designs for comparison with the pyramid configuration in terms of tracking errors.

References

[1] Wie, B., "Singularity Escape/Avoidance Steering Logic for Control Moment Gyro Systems," *Journal of Guidance, Control, and Dynamics*, Vol. 28, No. 5, Sept-Oct. 2005, pp. 948-956. DOI: 10.2514/1.10136

[2] Carpenter, M. D., and Peck, M. A., "Reducing Base Reactions with Gyroscopic Actuation of Space-Robotic Systems," *IEEE Transactions on Robotics*, Vol. 25, No. 3, Dec. 2009, pp. 1262-1270. DOI: 10.1109/TRO.2009.2032953

[3] Duda, K. R. et al., "The Variable Vector Countermeasure Suit (V2Suit) for Space Habitation and Exploration," *Frontiers in Systems Neuroscience*, Vol. 9, No. 55, 6 Apr. 2017, pp. 1-13. DOI: 10.3389/fnsys.2015.00055

[4] Li, D., and Vallery, H., "Gyroscopic Assistance for Human Balance," *International Workshop on Advanced Motion Control*, 25-27 Mar. 2012, pp. 1-6. DOI: 10.1109/AMC.2012.6197144

[5] Wong, T. C. F., and Hung, Y.S., "Stabilization of Biped Dynamic Walking Using Gyroscopic Couple," *IEEE International Joint Symposia on Intelligence and Systems*, 4-5 Nov. 1996, pp. 102-108. DOI: 10.1109/IJSIS.1996.565057

[6] Paradiso, J. A., "Global Steering of Single Gimballed Control Moment Gyroscopes using a Directed Search," *Journal of Guidance, Control, and Dynamics*, Vol. 15, No. 5, Sept-Oct. 1992, pp. 1236-1244. DOI: 10.2514/3.20974

[7] Zhang, J., Ma, K., Meng, G., and Tian, S., "Spacecraft Maneuvers via Singularity-Avoidance of Control Moment Gyros based on Dual-Mode Model Predictive Control," *IEEE Transactions on Aerospace and Electronic Systems*, Vol. 51, No. 4, Oct. 2015, pp. 2546-2559. DOI: 10.1109/TAES.2015.130715

[8] Margulies, G., and Aubrun, J.N., "Geometric Theory of Single-Gimbal Control Moment Gyro Systems," *Journal of the Astronautical Sciences*, Vol. 26, No. 2, 1978, pp. 159-191.

[9] Kurokawa, H., "Survey of Theory and Steering Laws of Single-Gimbal Control Moment Gyros," *Journal of Guidance, Control, and Dynamics*, Vol. 30, No. 5, Sept. 2007, pp. 1331-1340. DOI: 10.2514/1.27316

[10] Schaub, H., Vadali, S. R., and Junkins, J. L., "Feedback Control Law for Variable Speed Control Moment Gyros," *Journal of the Astronautical Sciences*, Vol. 46, No. 3, July-Sept. 1998, pp. 307-328.

[11] Bedrossian, N. S., Paradiso, J., Bergmann, E. V., and Rowell, D., "Steering Law Design for Redundant Single-Gimbal Control Moment Gyroscopes," *Journal of Guidance, Control, and Dynamics*, Vol. 13, No. 6, Nov-Dec. 1990, pp. 1083-1089. DOI: 10.2514/3.20582

[12] Ford, K. A., Hall, C. D., "Singular Direction Avoidance Steering for Control-Moment Gyros," *Journal of Guidance, Control, and Dynamics*, Vol. 23, No. 4, July-Aug. 2000, pp. 648-656. DOI: 10.2514/2.4610

[13] Bedrossian, N. S., Paradiso, J., Bergmann, E. V., and Rowell, D., "Redundant Single Gimbal Control Moment Gyroscope Singularity Analysis," *Journal of Guidance, Control, and Dynamics*, Vol. 13, No. 6, Nov-Dec. 1990, pp. 1096-1101. DOI: 10.2514/3.20584

[14] Cornick, D. E., "Singularity Avoidance Control Laws for Single Gimbal Control Moment Gyros," *AIAA Guidance and Control Conference*, AIAA, New York, 1979, pp. 255-267. DOI: 10.2514/6.1979-1698

[15] Vadali, S.R., Oh, H.S., and Walker, S.R., "Preferred Gimbal Angles for Single Gimbal Control Moment Gyros," *Journal of Guidance, Control, and Dynamics*, Vol. 13, No. 6, Nov-Dec. 1990, pp. 1090-1095. DOI: 10.2514/3.20583

[16] Takada, K., Kojima, H., and Matsuda, N., "Control Moment Gyro Singularity-Avoidance Steering Control Based on Singular-Surface Cost Function," *Journal of Guidance, Control, and Dynamics*, Vol. 33, No. 5, Sept-Oct. 2010, pp. 1442-1450. DOI: 10.2514/1.48381

[17] Leve, F. A., Munoz, J. D., and Fitz-Coy, N. G., "Gimbal-Lock Escape via Orthogonal Torque Compensation," *AIAA Guidance, Navigation, and Control Conference*, 3 Aug. 2010, pp. 1-10. DOI: 10.2514/6.2010-8069

[18] Wie, B., Bailey, D., and Heiberg, C., "Singularity Robust Steering Logic for Redundant Single-Gimbal Control Moment Gyros," *Journal of Guidance, Control, and Dynamics*, Vol. 24, No. 5, Sept-Oct. 2001, pp. 865-872. DOI: 10.2514/2.4799

[19] Yamada, K., and Jikuya, I., "Directional passability and quadratic steering logic for pyramid-type single gimbal control moment gyros," *Acta Astronautica*, Vol. 102, 2014, pp. 103-123. DOI: 10.1016/j.actaastro.2014.05.022

[20] Berry, A., Lemus, D., Babuska, R., and Vallery, H., "Directional Singularity-Robust Torque Control for Gyroscopic Actuators," *IEEE/ASME Transactions on Mechatronics*, Vol. 21, No. 6, 2016, pp. 2755-2763. DOI: 10.1109/tmech.2016.2603601

[21] Chiaverini, S., "Singularity-Robust Task-Priority Redundancy Resolution for Real-Time Kinematic Control of Robot Manipulators," *IEEE Transactions on Robotics and Automation*, Vol. 13, No. 3, 1997, pp. 398-410. DOI: 10.1109/70.585902

[22] Oh, H.S., and Vadali, S.R., "Feedback Control and Steering Laws for Spacecraft using Single Gimbal Control Moment Gyros," *Guidance, Navigation, and Control Conference*, 14 Aug. 1989, pp. 420-430. DOI: 10.2514/6.1989-3475

[23] Maciejewski, A. A., and Klein, C. A., "Numerical Filtering for the Operation of Robotic Manipulators through Kinematically Singular Configurations," *Journal of Robotic Systems*, Vol. 5, No. 6, Dec. 1988, pp. 527-552. DOI: 10.1002/rob.4620050603

[24] Wie, B., "New Singularity Escape/Avoidance Steering Logic for Control Moment Gyro Systems," *AIAA Guidance and Control Conference*, Austin Texas, 11-14 Aug. 2003, pp. 1-11. DOI: 10.2514/6.2003-5659